Published in Solar Energy
Volume 199, 15 March 2020, Pages 377-399
https://doi.org/10.1016/j.solener.2020.02.044

Performance assessment of BIPV/T double-skin façade for various climate zones in Australia: effects on energy consumption

Siliang Yang[1], Alessandro Cannavale[2], Aldo Di Carlo[3], Deo Prasad[4], Alistair Sproul[5], Francesco Fiorito[1,6,*]

[1] Faculty of Built Environment, University of New South Wales, Sydney, Australia

[2] Department of Sciences in Civil Engineering and Architecture, Polytechnic University of Bari, Bari, Italy

[3] Department of Electronics Engineering, University of Rome "Tor Vergata", Rome, Italy

[4] Cooperative Research Centre for Low Carbon Living, Sydney, Australia

[5] School of Photovoltaic and Renewable Energy Engineering, University of New South Wales, Sydney, Australia

[6] Department of Civil, Environmental, Land, Building Engineering and Chemistry, Polytechnic University of Bari, Bari, Italy

* corresponding author. francesco.fiorito@poliba.it, +390805963401

Abstract

As the sub-system which constitutes the interface between indoor and outdoor, building envelope significantly influences indoor heating and cooling loads and thus affects building energy consumption. This paper presents the results of an experimental analysis involving numerical simulation for the performance prediction of building-integrated photovoltaic/thermal double-skin facade (BIPV/T-DSF). Different BIPV materials (amorphous silicon PV, dye-sensitized solar cell, and Perovskite based solar cells) have been considered as the exterior cladding of a North-facing facade of an office building located in Australia. The performance assessment has involved the selection of three climates across Australia, represented by the cities of Darwin, Sydney and Canberra. The air cavity created between the outer skin and the inner one has been alternatively assessed in the non-ventilated, naturally-ventilated and mechanically-ventilated mode of operation, while a full sensitivity analysis was performed in order to assess the influence of different design parameters, such as internal skin's thermal transmittance, cavity depth, ventilation louvres' size, and cavity ventilation rate. By comparing the different operational modes and different BIPV technologies, it was found that mechanically-ventilated DSF integrating the Perovskite-based solar cell could be the optimal configuration achieving the best energy savings in comparison to traditional technologies. In addition to the reduction of building's heating and cooling loads, this technology can harvest electrical energy – converted at an almost constant rate throughout the entire year – and thermal energy due to the increased air temperature within the cavity. The study has, finally, demonstrated, that the harvested energy could cover a significant share of building's energy consumption, almost compensating it for most of the year.

1. Introduction

Health and environmental issues have become a common concern for people all over the world. Along with the rapid progress of urbanization and growth of population, the world energy consumption has increasingly raised. This leads to the exhaustion of energy resources and heavy environmental impacts [1]. Building sector contributes to approximately one third of the total energy consumption in most countries [2], while in developed countries residential and commercial buildings consume between 20% and 40% of the total energy. As a consequence, the energy consumption in building sector now exceeds the one of the other major sectors such as industry and transportation [1]. In Australia, the total energy consumption of commercial buildings accounts for roughly 10% of the nation's overall energy consumption, whilst 25% of this total come from commercial office buildings [3, 4]. Energy consumption due to the conditioning of indoor spaces constitutes the largest proportion of this consumption [4].

As the sub-system at the interface between indoor and outdoor, the building envelope, controlling thermal fluxes exchanged by the building, significantly influences indoor spaces' heating and cooling loads, therefore affecting building energy consumption [5]. However, many conventional building facades are not able to implement good energy and thermal performance [6]. In this context, it is important to explore high performance façades for commercial buildings to improve energy efficiency. In general, the various high-performance façade technologies of buildings are based on the capabilities to control at the same time daylight, solar gain, thermal exchange and ventilation, in order to enhance indoor comfort and to limit the use of Heating, Cooling and Air Conditioning (HVAC) systems [7]. Double-Skin Façade (DSF) is one proved solution integrating the previously described four functions. This is due to the presence of a ventilating cavity and operable vents, which increase thermal insulation while maintaining acceptable daylighting and ventilation for the building [8]. The DSF consists of an external transparent skin, which protects the internal façade, creating a ventilating air cavity in between the two skins. Operable ventilation louvres complete the system and connect the air cavity with both the outdoor and the indoor space [9]. Earlier, several studies have found that closing the DSF's cavity in the winter period minimizes heat losses, hence decreasing the building heating consumption [10-14]. On the contrary summer cooling consumption can be reduced by opening the external louvres and introducing fresh air in the ventilated cavity; this operation removes unwanted heat by means of the thermal buoyancy driven ventilation [11-15].

The ventilation of the air cavity produces a positive effect of "thermal washing" (i.e. the reduction of the surface temperature of the building components in contact with the air cavity), which is particularly beneficial when Photovoltaic (PV) systems are integrated in the outer layer of the façade [16-18]. Together with the increase of the PV efficiency due to the decrease of the PV layer surface temperature, the collection of unwanted hot air is another beneficial opportunity of such as this system, which is yet not totally exploited. Looking at this system from another perspective, the entire façade becomes a large Building-Integrated Photovoltaic/Thermal (BIPV/T) system.

Although PVT systems [19-21] and solar thermal systems [22] have demonstrated to be a viable solution for the production of electrical energy or of useful thermal energy when integrated into building envelope [23-28], the combination of DSF and BIPV/T technology deserves to be further explored and is the object of our study. Several performance assessment studies of BIPV/T-DSF facades are already reported in the recent literature [29, 30]. Joe et al. [31] studied a multi-story DSF building integrated with spandrel poly-crystalline BIPV panel (BIPV-DSF) in South Korea. They found that the BIPV-DSF reduces of about respectively 16% and 7% the heating and cooling energy consumption, in comparison to single-skin façades (SSF). The authors analysed the overall heating and cooling consumption, but the assessment of the amount of collected thermal energy was outside the scope of the study. Peng et al. [32] compared the thermal performance of a building equipped between a normal DSF and with monocrystalline silicon BIPV-DSF. The results of the analysis, performed in Hong Kong by means of numerical simulation, showed that the BIPV-DSF could reduce heat gain by 51% in summer and heat loss by 32% in winter. A similar result in terms of reduction of building total energy consumption (51% reduction recorded) by using a BIPV-DSF instead of a clear DSF was found by Peng et al. [33]. BIPV/T-DSF are not only useful in reducing heating and cooling load, but also to provide useful thermal and electrical energy. The amount of this energy could be relevant, which was also pointed out by Ioannidis et al. [34], who performed a thermal and energy analysis of a high-rise office building in Montreal (Canada). The authors found that, when a semi-transparent BIPV-DSF was used, the annual total solar electricity produced by the facade was almost meeting the heating and cooling consumption of the interior perimeter zones of the building. Although BIPV-DSF consistently show benefits with respect to the reduction of total energy consumption in comparison to other traditional façade technologies, BIPV-DSF solar conversion performance is highly affected by the air cavity ventilation mode, by the climate and by the transparency of the PV panel. Peng et al. [35] found, indeed, that a ventilated BIPV-DSF produces 3% more electric power than the non-ventilated BIPV-DSF since the ventilation in the cavity provided lower operating temperature for the PV panel. Saadon et al. [30] conducted a simulation study for an office building using BIPV/T-DSF system in different climate zones in France, reported that the higher electrical and thermal efficiency of the BIPV/T-DSF system was achieved in warmer climates; it was also found that the electrical efficiency of opaque PV/T panel was much higher than the one of semi-transparent PV/T panel, and the PV/T electrical efficiency decreased with the increase of PV transparency. Elarga et al. [36] found that the thermal and electrical performance of BIPV-DSF was highly affected by the ventilation mode in the cavity, especially when additional thermal mass – in their study provided by means of the integration of phase-change materials (PCMs) into the system – was introduced. The authors found that the use of PCMs contributed in further reducing the building's total energy consumption by an additional 20% to 30% by shifting the release of heat within the air cavity. In this last case, however, the performances are highly affected by the thermal properties of selected PCMs.

Although several studies are reported in literature on the benefits due to the adoption of BIPV-DSF, limited researches are available on the numerical analysis of the combined influence of climate and PV transparency on BIPV-DSF performance. Moreover, few studies reported the benefits due to the exploitation of useful thermal energy collected by BIPV/T-DSF. For this purpose, in this paper, thermal and electrical performance of commercial buildings configured with semi-transparent BIPV/T-DSF under a range of climatic conditions in Australia was investigated. In addition, the performances of BIPV/T-DSF using different types of semi-transparent PV/T glazing were compared thoroughly.

2. Methods

The research questions presented in the previous paragraph were answered by using numerical simulations of the thermal and electrical performance of a BIPV/T-DSF integrated onto a reference building. The reference building reflects the dimensions and characteristics of a real-scale application developed by Peng et al. and presented in [35, 37]. In this way it has been possible to calibrate the numerical model against real-time measurements collected during the experiments and reported in the literature [38, 39]. The reference model is representative of a single-room building of 2.3 m of length, 2.44 m of width, and 2.47 m of height. Three of the four external walls – specifically the ones exposed to the south, east and west – have been modelled as adiabatic, thus representing a typical intermediate room in a cellular office building. The fourth wall (i.e. the one exposed to the north) has been modelled with four configurations to reflect different typologies and modes of operation of BIPV/T-DSF:

- Model (1): BIPV/T single-skin façade (SSF). This façade is considered as the benchmark case for the performance comparison of the other three models. The façade consists of a window of 6 m^2 of surface, of which 3 m^2 semi-transparent and 3 m^2 opaque (constituting the spandrel and the upper portion of the façade). The semi-transparent portion of the façade consists of a window (thermal-break aluminium frame) embodying a PV panel integrated into a Single-Glazing Unit (SGU). Three different semi-transparent PV panels were tested as described in the following paragraph and the thermal and visual properties of the overall window – Visible Light Transmittance (VLT), thermal transmittance (U-value) and solar transmittance – are given in

- Table *1*. The thermal properties of the opaque portion of the external wall are given in Table 2 and reflect the typical thermal properties of the external envelope of an office building compliant with local regulations – Section J of the Australian National Construction Code for the selected climate zones [40].
- Model (2): non-ventilated BIPV/T-DSF. This model represents the simplest mode of operation of a BIPV/T-DSF. As shown in Fig. 1, the façade consists of two skins (each composed of an SGU window) with a 0.4 m air cavity in between the two. Each of the two skins has an opaque portion (upper and lower) which represents in the reality the ventilation louvre in the closed position. The air cavity is neither in contact with the outdoor air nor with the indoor room and serves only as thermal buffer between the two spaces. Therefore, no hot air is extracted from the air cavity.
- Model (3): naturally-ventilated BIPV/T-DSF. The façade has the same geometrical properties as the previous model. The only difference is that the cavity in between the two skins is in direct contact with the outdoor air by means of two operable louvres. The louvres have a dimension of 2.32 m x 0.5 m and follow the specifications of commercially available products [41]. In the numerical model of the external louvres, a discharge coefficient (the ratio of the actual airflow to the theoretical airflow) of 0.39 has been used. In Model (3) both the internal window and the internal louvres have been kept closed, so that no air exchange happens between the cavity and the room.
- Model (4): mechanically-ventilated BIPV/T-DSF. The façade has the same geometrical properties as Model (2) and Model (3). The only difference is that the air cavity is mechanically ventilated at a constant rate by means of a fan. In this case, a constant airflow rate of 400 air changes per hour (ACH) was assumed, as per previously published studies [42].

For models (3) and (4), in addition to the determination of the heating and cooling energy consumption and of the electricity production from the PV panel, the results presented in the following paragraph include the calculation of the ideal thermal energy (Q), as defined below [43]:

$$\boldsymbol{Q} = \int \dot{\boldsymbol{Q}} \times \boldsymbol{dt} \quad [\boldsymbol{Wh}] \tag{1}$$

where

$$\dot{\boldsymbol{Q}} = \dot{\boldsymbol{m}} \boldsymbol{c_p} \left(\boldsymbol{T_{flow,out}} - \boldsymbol{T_{flow,in}} \right) [\boldsymbol{W}] \tag{2}$$

and $\dot{m}$ represents the mass flow rate (kg/s) of the airflow through the cavity of the double-skin façade; c_p represents the specific heat capacity of the air in the cavity (J/kg °C); while $T_{flow,out}$ and $T_{flow,in}$ (°C) represent respectively the temperature of the air exiting and entering the cavity.

We assumed that during cool indoor conditions, the ideal thermal energy was used to reduce the heating load of the room, while during warm indoor conditions, the ideal thermal energy was used to provide cooling load to the room by means of a desiccant cooling system (DSCS).

In this last case, we assumed a thermal COP of the DSCS, calculated according to eq. 3 [44], equal to 0.9.

$$\boldsymbol{COP} = \frac{\boldsymbol{Q_{cooling}}}{\boldsymbol{Q_{solar\ thermal}}} \quad (3)$$

Therefore, the useful portion Q_u of the ideal thermal energy Q can be defined as follows:

$$\begin{cases} Q_u = Q|_{heating\ season} \\ Q_u = Q \times COP|_{cooling\ season} \end{cases} \quad (4)$$

Fig. 1 presents the schematic diagram of the four building models. Semi-transparent PV glazing, as the external window glazing, was applied to all the models. Three types of semi-transparent PV glazing with comparable VLT were selected for the study (

Table *1*). The selected VLT values of the PV glazing were within the range of 25% - 38%, which is based on previous studies [45], and have been determined as suitable for controlling both daylighting and solar gains through external windows. As such, the energy usage of artificial lighting for the four models was assumed to be the same.

Table 1. Properties of the semi-transparent PV glazing.

PV Type	**Perovskite PV**	**Amorphous Silicon PV (a-Si)**	**Dye-sensitized solar cell (DSC)**
Source	[46, 47]	Onyx Solar Energy S.L.	[48]
U-value (W/m^2K)	5.59	5.14	5.39
Visible Light Transmittance (VLT)	37.5%	27.0%	25.0%
Solar Transmittance (front)	33.2%	18.6%	33.5%
Solar Transmittance (back)	33.2%	18.6%	33.5%
Solar Reflectance (front)	3.5%	9.0%	10.1%
Solar Reflectance (back)	3.5%	28.5%	10.1%
Visible Light Reflectance (front)	4.0%	7.1%	7.2%
Visible Light Reflectance (back)	4.0%	34.3%	7.2%
Emissivity	0.89	0.84	0.84
PV efficiency (under STC), η (%)	6.64	2.84	3.5
Temperature coefficient of power (%/°C)	-0.3	-0.19	-0.2

Table 2. Thermal properties of building envelope for simulations.

Parameters	Model (1)	Model (2)	Model (3)	Model (4)
U-value of external wall (W/m^2K)	0.51	0.51	0.51	0.51
U-value of external roof (W/m^2K)	0.316	0.316	0.316	0.316
U-value of internal window (W/m^2K)	N/A	5.68	5.68	5.68

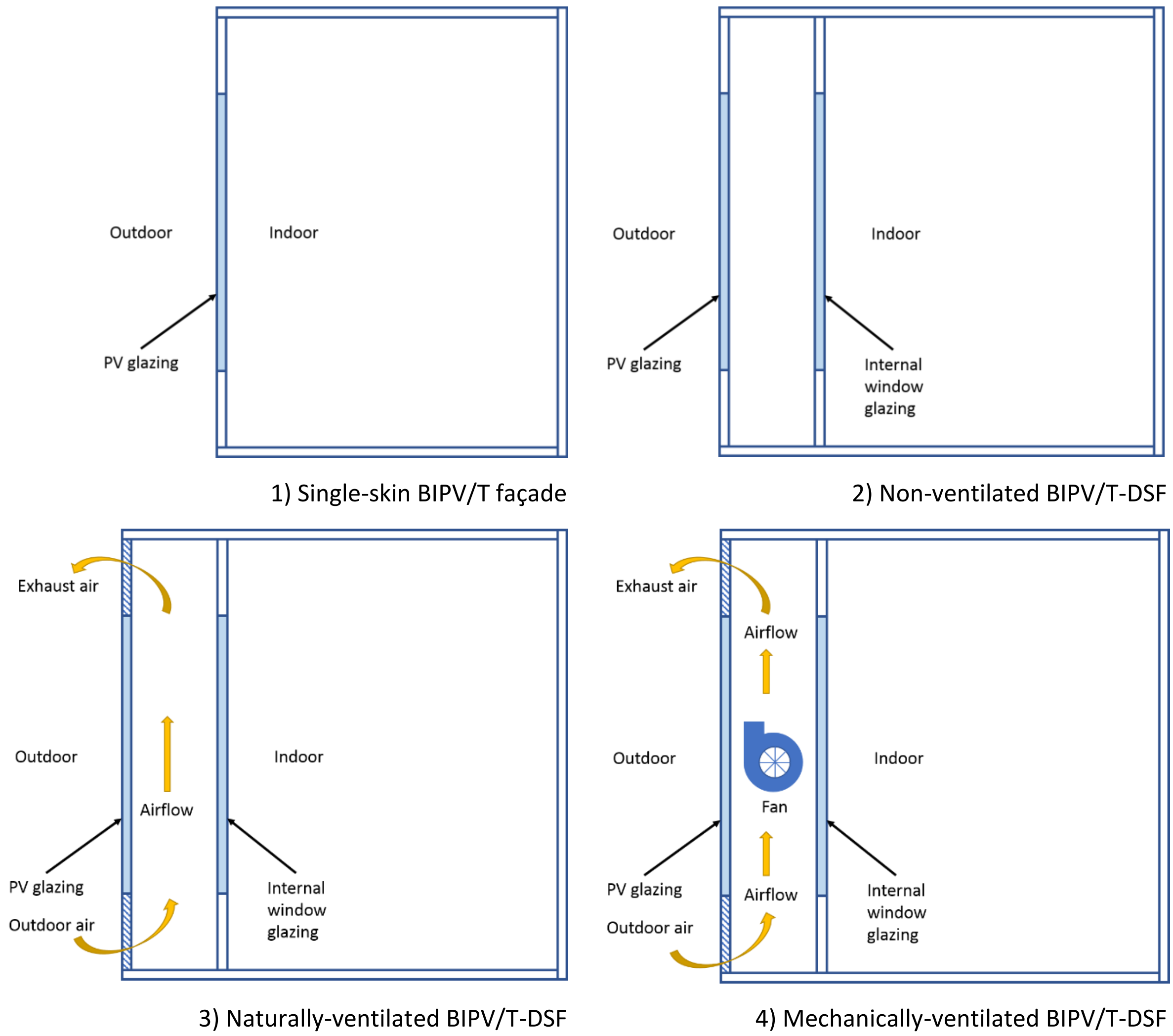

Fig. 1: Schematic diagram of the four façade/building models.

TRNSYS and TRNFlow simulation software were used to model the building with the four corresponding façade systems. TRNSYS is a graphically based software which has already been validated and widely used in BIPV research studies [38, 39, 49-52]. The cooling and heating consumption of the building as well as the electricity production of the PV/T system were directly calculated in TRNSYS. TRNFlow is an external engine for TRNSYS which aids the calculation of natural ventilation [53], and this was integrated into the TRNSYS thermal building model (Type56) for analysing the performance of the natural ventilation within the DSF. As specified in previous studies [52], the opening louvres of the naturally-ventilated DSF cannot be directly modelled in either TRNSYS or TRNFlow. Thus, louvres were modelled as windows with internal blinds, whereas the opening ratio was implemented by modulating the discharge coefficient, as described in earlier.

Three different Australian climate zones (i.e. Darwin, Sydney and Canberra) were selected, whose characteristics are reported in

Table 3. This decision was made in order to compare the results of the current study with the one presented in the previously published study which examined the same three climates [52]. Standard climatic files, from the International Weather for Energy Calculations (IWEC) database were used in the TRNSYS simulations. Fig. 2 shows the TRNSYS model with all the linked types.

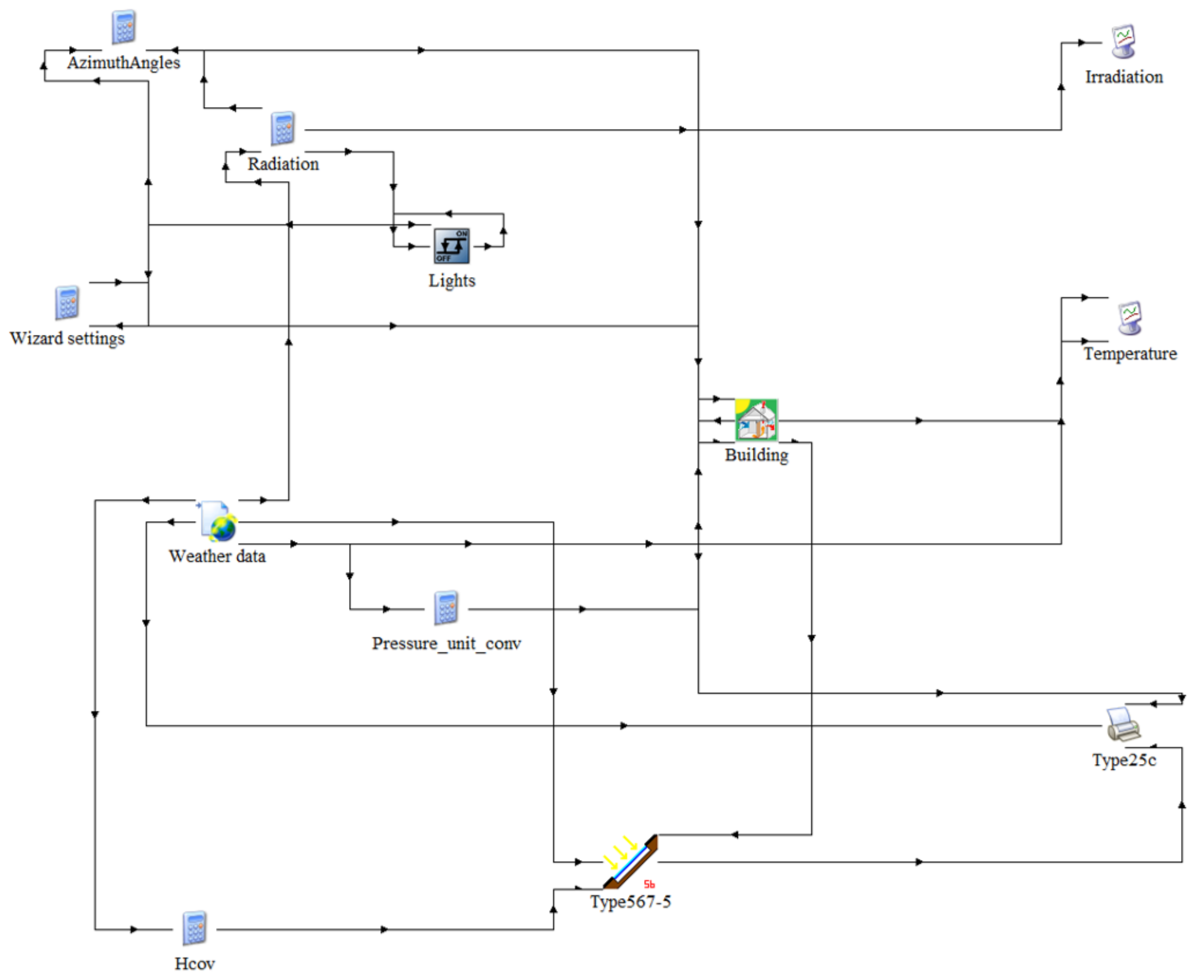

Fig. 2: Schematic diagram of the façade/building model in TRNSYS.

Table 3. Description of the climate zones used for the simulations.

Location	Brief description of the climate zone based on Australian Building Codes Board	Brief description of the climate zone based on Koppen-Geiger climate classification
Darwin	High humidity summer & warm winter	Tropical savanna climate
Sydney	Warm temperate	Humid subtropical climate
Canberra	Cool temperate	Oceanic climate

Typical office building operating hours and internal gains were applied to the building simulations for all the models and these are specified in

Table 4. A reversible heat pump system was considered to provide heating and cooling for the building with a heating COP of 3.5 and cooling COP of 2.5 [54]. Indoor temperature setpoints for heating and cooling were set at 22°C and 26°C respectively.

Table 4. Building internal gains for the operating schedule and TRNSYS simulations.

Item	All models
Operating schedule	8am to 6pm
Heat gain from persons	0.15 kW
Heat gain from computers	0.14 kW
Heat gain from artificial lightings	5 W/m^2

Item	All models
Operating schedule	8am to 6pm
Heat gain from persons	0.15 kW
Heat gain from computers	0.14 kW
Heat gain from artificial lightings	5 W/m^2

3. Model calibration and sensitivity analysis

In order to achieve accurate and reliable results of the simulation, a set of TRNSYS test models were created and calibrated against published experimental data. The TRNSYS models (2) – non-ventilated BIPV/T-DSF – and (3) – naturally-ventilated BIPV/T-DSF – were calibrated against real-time experimental results [33, 35, 37]. The major parameters affecting the accuracy of the simulation results, such as equipment and occupancy schedule, thermal properties of the building envelope, internal gains and other operational settings were fine-tuned to match the experimental results within an acceptable level of accuracy. For the model (2), the BIPV back surface temperature and indoor air temperature were selected as control variables for the calibration. For the model (3), the BIPV back surface temperature and internal window back surface temperature were selected as control variables for the calibration. According to ASHRAE [55], hourly mean bias error (MBE) and cumulative variation of root mean squared error (CVRMSE), derived from the comparison of measured and simulated values of the selected control variables, were used as indices for the calibration. Results of the calibration process are given in Table 5.

The MBE was calculated according to the following formula [55]:

$$\boldsymbol{MBE} = \frac{\sum_{i=1}^{Np}(M_i - S_i)}{\sum_{i=1}^{Np} M_i} \quad (5)$$

where M_i and S_i are the measured and simulated data and N_p denotes the total number of values considered for a particular period of time.

The CVRMSE was calculated according to the following formula [55]:

$$CVRMSE_{(P)} = \frac{\sqrt{\sum_{i=1}^{N_P}((M_i - S_i)^2/N_P)}}{\overline{M_P}} \quad (6)$$

where $\overline{M_p}$ is the average of the measured values. The calibrations were deemed to be acceptable if the MBE was within ±10%, and the CVRMSE was less than 30%.

Table 5. Results of the calibration of the TRNSYS models [38, 39, 52].

Operation mode	Parameter to be calibrated	MBE	CVRMSE	Met hourly acceptance criteria?
Model (2)	PV back surface temperature	4.55%	14.48%	Yes
Model (2)	Indoor air temperature	-1.02%	5.5%	Yes
Model (3)	PV back surface temperature	2.76%	12.67%	Yes
Model (3)	Internal window back surface temperature	-3.03%	5.95%	Yes

In addition, a sensitivity analysis was carried out to thoroughly understand how the building's total energy consumption was sensitive to the variation of geometrical and thermal parameters of the model. The goal was to optimize the model's energy predictions by examining the parameters which show the highest sensitivity in the model. To this extent we decided to perform the parametric analysis on the model with a-Si PV panels for the climate of Sydney. We selected as control parameters the thermal transmittance of the internal window, the depth of the air cavity, the louvres' discharge coefficient in the naturally ventilated model, as well as the airflow rate of the fan in the mechanically ventilated model.

Results of the sensitivity analysis performed on models (2), (3), and (4) are shown respectively in Fig. 3, Fig. 4, and Fig. 5. As it can be seen from the figures, all models appear to be highly sensitive to the variation of the thermal transmittance of the internal window. However, this parameter has a different effect on the non-ventilated model – (2) and on ventilated models – (3) and (4). Note that for the non-ventilated model a reduction of the window's thermal transmittance produces a decrease of the total energy consumption, a similar variation of this control parameter in the other two models produces an opposite effect. Looking at the details of the results of the sensitivity analysis carried out on model (2) and shown in Fig. 3, it can be seen that a reduction of 80% of the window's thermal transmittance produces a reduction of the total energy consumption of the reference room by about 15%. Note also, that for model (2), the change in total energy consumption has an almost linear relationship with the change of the internal window's thermal transmittance.

The variation of depth of the non-ventilated air cavity has a lower influence on the energy consumption in comparison with the previous control parameter. Also, in this case, it can be noticed an almost linear relationship between increase or decrease of the cavity depth and respectively decrease or increase of total energy consumption, with a rate of about 1.5% of variation of total energy consumption for each 10% of variation of cavity depth (see Fig. 3).

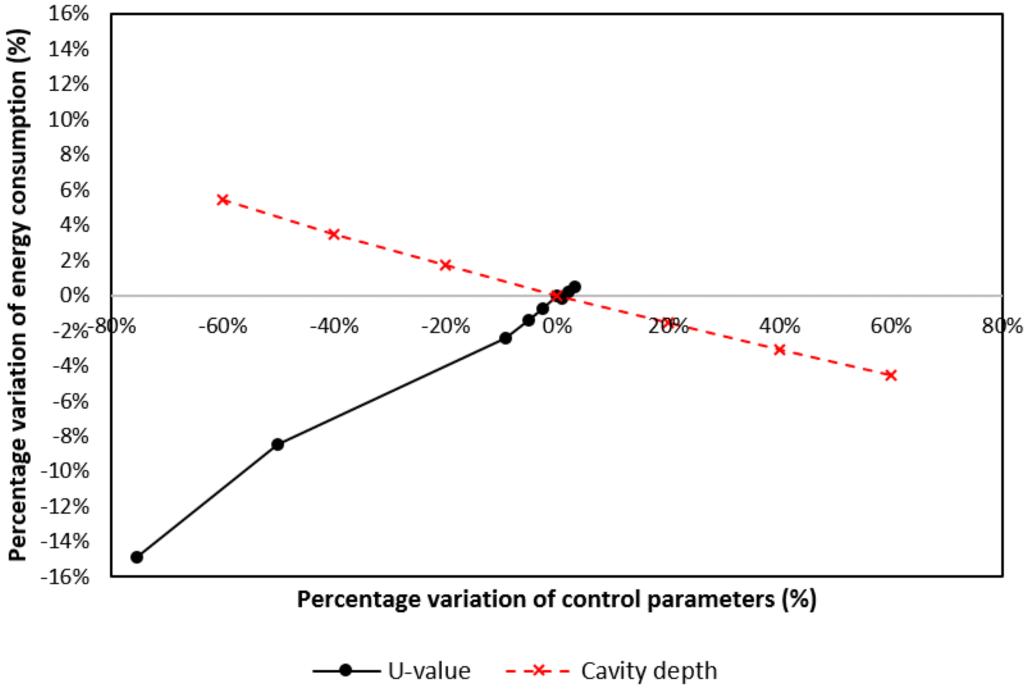

Fig. 3: Sensitivity analysis of model (2)

Fig. 4 shows the results of the sensitivity analysis applied to the naturally-ventilated model. In this case, the model is more sensitive to the discharge coefficient than to the other two control parameters. As a matter of fact, a variation of 10% of the discharge coefficient produces a variation of about 0.8% of the total annual energy consumption, which is almost double the variation obtained with a change in the cavity depth. Also note that the change of the window's thermal transmittance produces a bifold effect, depending on whether a SGU or a Double-Glazing Unit (DGU) is adopted. For variations of the internal window's thermal transmittance lower than 10% (still corresponding to the use of an SGU) this produces a decrease of the total energy consumption. If, however, a DGU is adopted and the window's thermal transmittance is further reduced, an increase of total building's energy consumption is obtained.

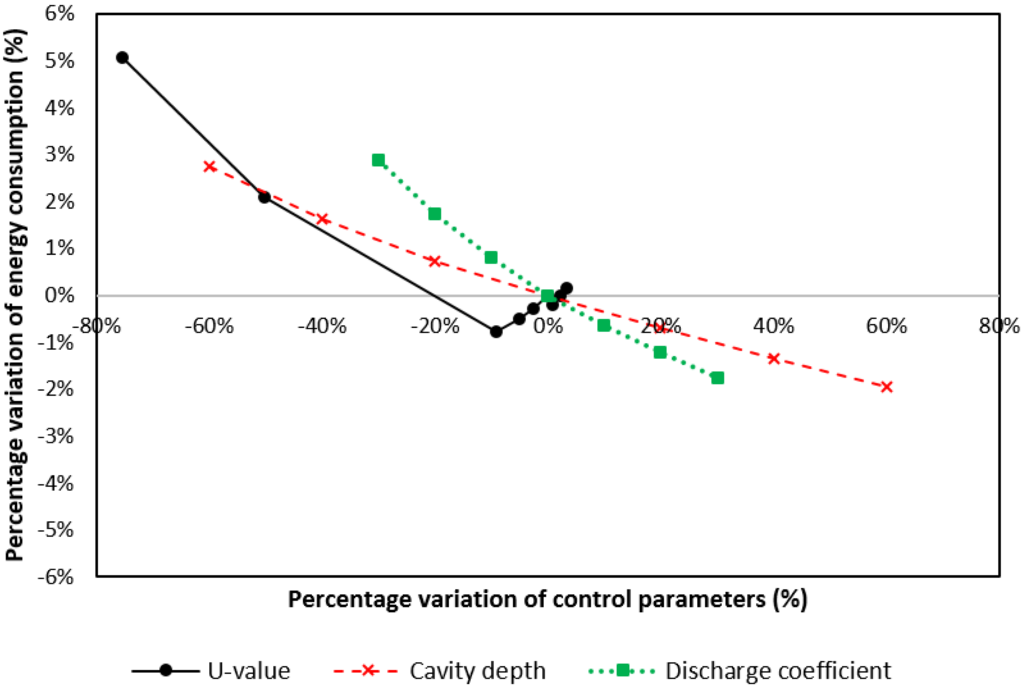

Fig. 4: Sensitivity analysis of model (3)

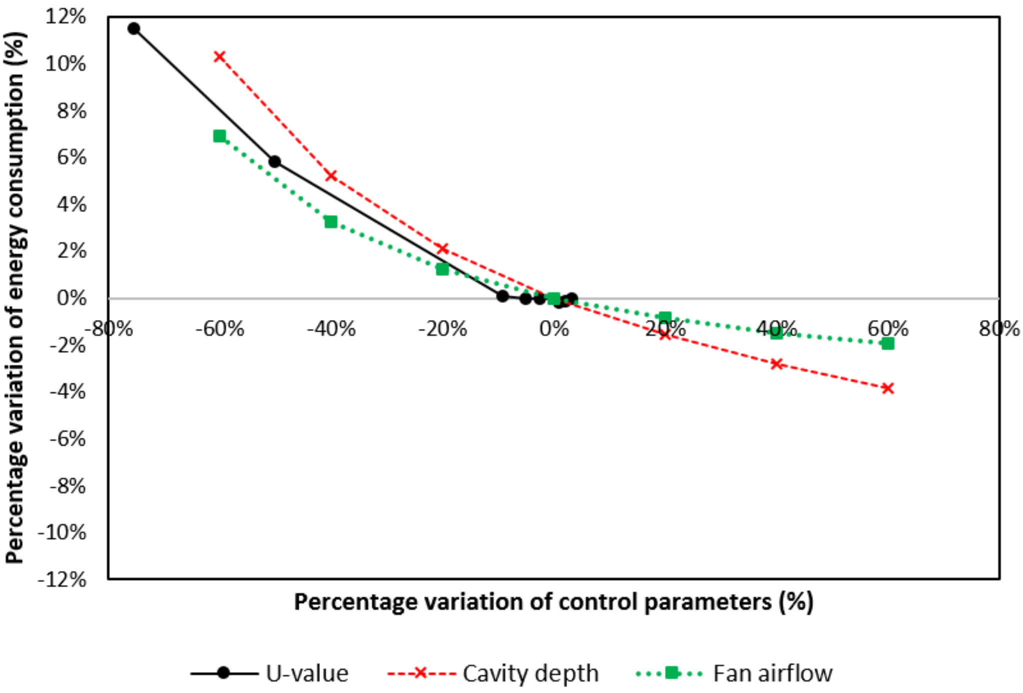

Fig. 5: Sensitivity analysis of model (4)

A similar trend is shown for the mechanically-ventilated model, whose sensitivity analysis is reported in Fig. 5. In this last case, however, the parameter affecting the most the total energy consumption is the cavity depth (as an average about 1.2% variation of total energy consumption for each 10% of variation of the control parameter), followed by window's thermal transmittance (as an average about 1% variation of total energy consumption for each 10% of variation of the control parameter) and finally followed by fan airflow rate (as an average about 0.8% variation of total energy consumption for each 10% of variation of the control parameter). The variations of all three control parameters produce a similar effect: a reduction of the values of the control parameter produces an increase of the total energy consumption.

4. Results

4.1 Energy performance and PV production

In this section, the energy performance of the different models previously described is presented. The results included in the following figures are grouped for climatic area. Since the scope of the analysis is to compare the energy performances of the different models, the results include only heating and cooling energy consumption, together with the energy converted by the PV system. Therefore, consumptions of electricity for lighting and for office equipment are excluded from the analysis, not being affected by the PV type or by the façade's mode of operation.

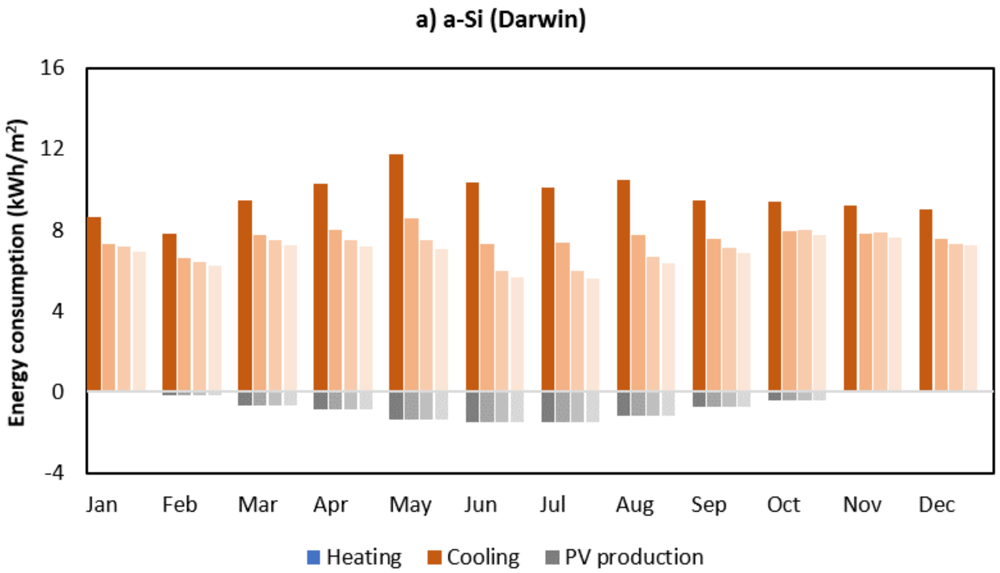

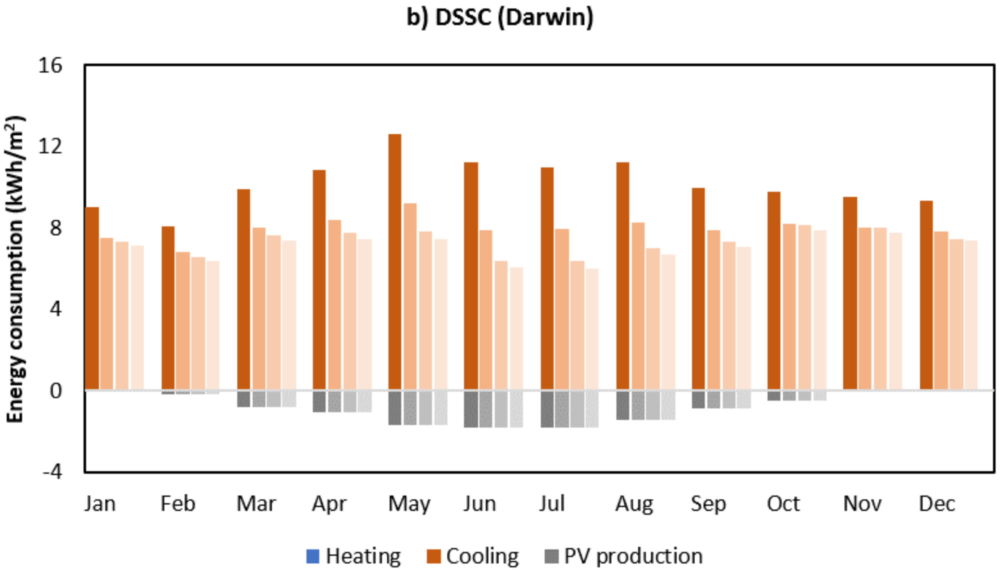

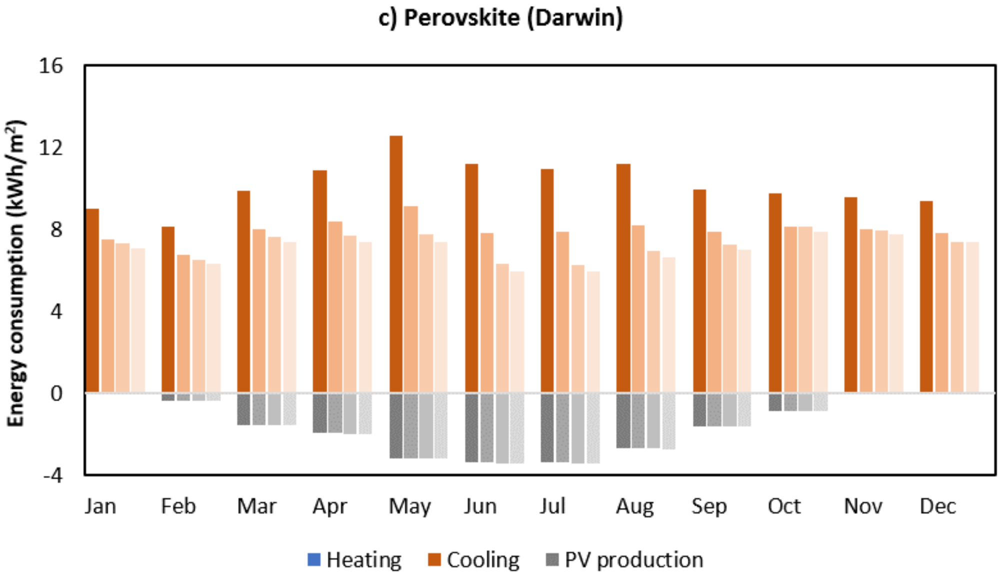

Fig. 6 a), b) and c): Energy consumption and PV production for three different PV glazing throughout the year in Darwin.

Fig. 6 shows the results of the energy analysis performed on the four models in Darwin. Each set of bars represents the monthly value of heating (blue) and cooling (orange) energy consumption, and of energy production from PVs (grey) for the four models. The colour of the bars varies from dark to pale moving from model (1) to model (4). In the hot tropical climate, as predictable, the heating energy consumption is almost zero, while the cooling energy consumption is almost stable over the year, variable from 7.79 kWh/m^2 month and 12.63 kWh/m^2 month for model (1) and from 5.58 kWh/m^2 month and 9.20 kWh/m^2 month for models integrating a DSF (2, 3, and 4). Conversion of energy from PV is mainly concentrated in the period between March and October, with peaks in the months of May, June and July. The production of PV energy shows a limited variability with the change of the façade model, but is greatly affected by the PV type, with a peak monthly production of respectively about 1.47 kWh/m^2, 1.82 kWh/m^2, and 3.40 kWh/m^2 for a-Si, dye-sensitized, and perovskite-based solar cells. This is due to the higher power efficiency of perovskite-based solar cells in comparison with the other two types.

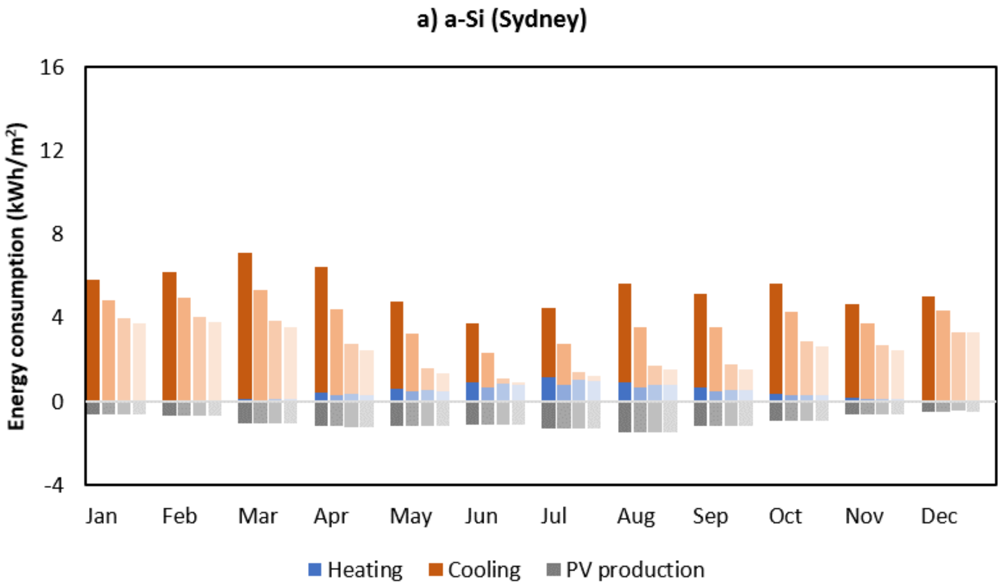

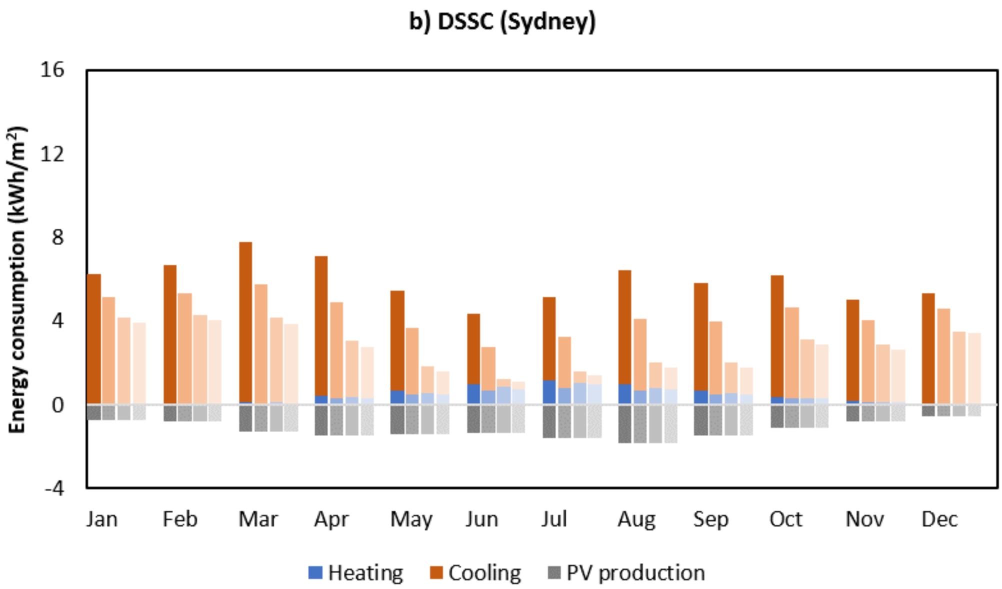

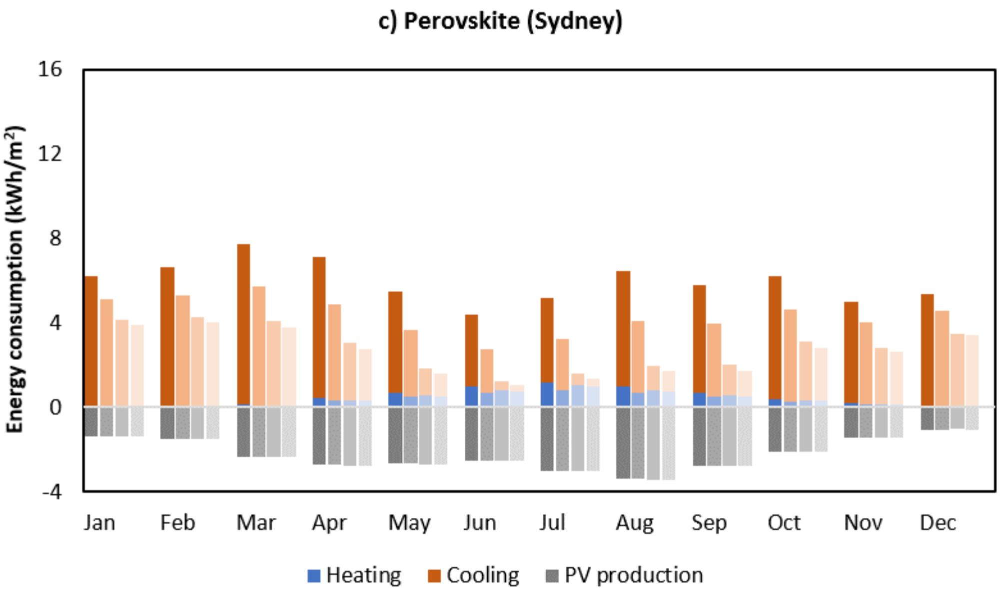

Fig. 7 a), b) and c): Energy consumption and PV production for three different PV glazing throughout the year in Sydney.

Fig. 7 includes the results of the energy analysis based on the warm temperate climatic region (represented by Sydney). As shown in the graphs, the pattern of heating and cooling energy consumptions is different from the one obtained for the tropical climate. In detail, distribution of cooling energy consumption is mainly concentrated in the hot months, with a peak during the month of March and the lowest value recorded in the month of June. It must be noticed that, as for the previous analysis, the model (1) has always a higher total energy consumption than the other 3 models and that ventilated facades – i.e. models (3) and (4) – always show positive benefits in terms of lower cooling and heating energy consumption and sometimes higher conversion rates of solar energy. Differently what recorded in tropical regions, the energy produced by the BIPV system is more uniformly distributed across the year, even though it still shows a peak at the end of the cold period (month of August). Monthly peak energy production is, also in this case, only slightly affected by façade's type, but is largely affected by PV type, with respectively a maximum monthly energy production of 1.86 kWh/m^2, 1.83 kWh/m^2 and 3.85 kWh/m^2 for a-Si, dye-sensitized, and perovskite-based solar cells.

Results of energy analysis performed in a cold temperate climate are reported in Fig. 8. The total energy consumption is always dominated by cooling energy consumption (variable in the range of 41 kWh/m^2 year and 47 kWh/m^2 year for the single-skin facade and of 13 kWh/m^2 year and 32 kWh/m^2 year for the double-skin façade), but heating energy consumption is significant in the cold months (between April and October), reaching a monthly peak values of about 2.5 kWh/m^2 in July. Production of electricity from BIPV is almost stable during the year and, depending on the PV type, reaches values of about respectively 12.5 kWh/m^2 year, 15.5 kWh/m^2 year, and 29.5 kWh/m^2 year for a-Si, dye-sensitized, and perovskite-based solar cells. These values, alone, fully cover and in some cases largely exceed the heating energy consumption of the building.

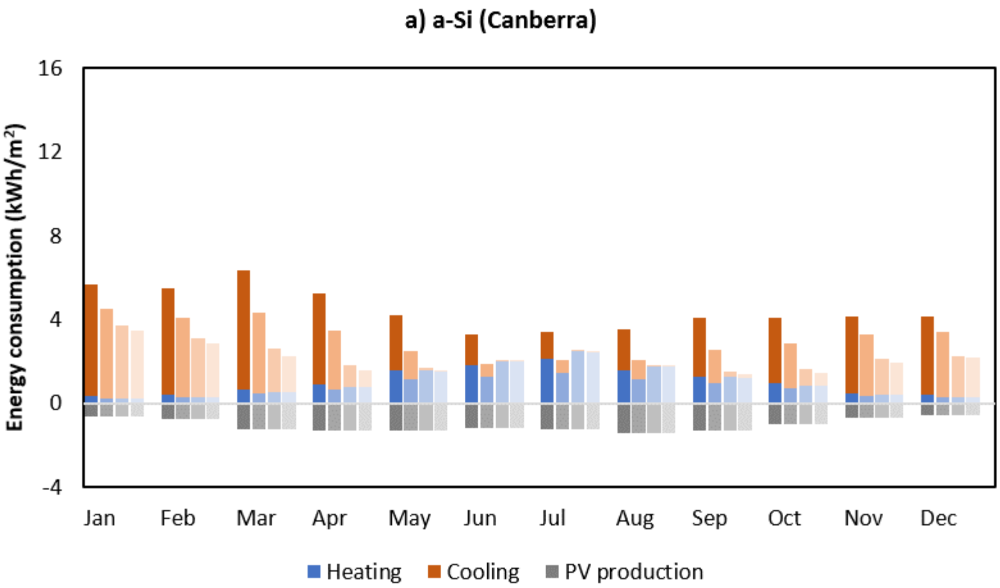
a) a-Si (Canberra)
Energy consumption (kWh/m²)
16
12
8
4
0
-4
Jan
Feb
Mar
Apr
May
Jun
Jul
Aug
Sep
Oct
Nov
Dec
Heating
Cooling
PV production

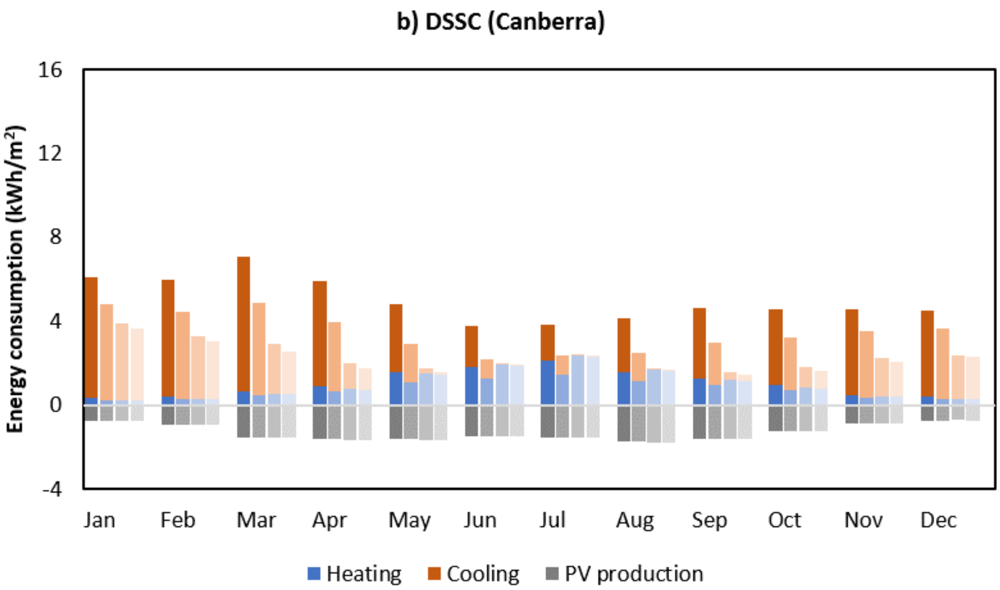
b) DSSC (Canberra)
Energy consumption (kWh/m²)
16
12
8
4
0
-4
Jan
Feb
Mar
Apr
May
Jun
Jul
Aug
Sep
Oct
Nov
Dec
Heating
Cooling
PV production

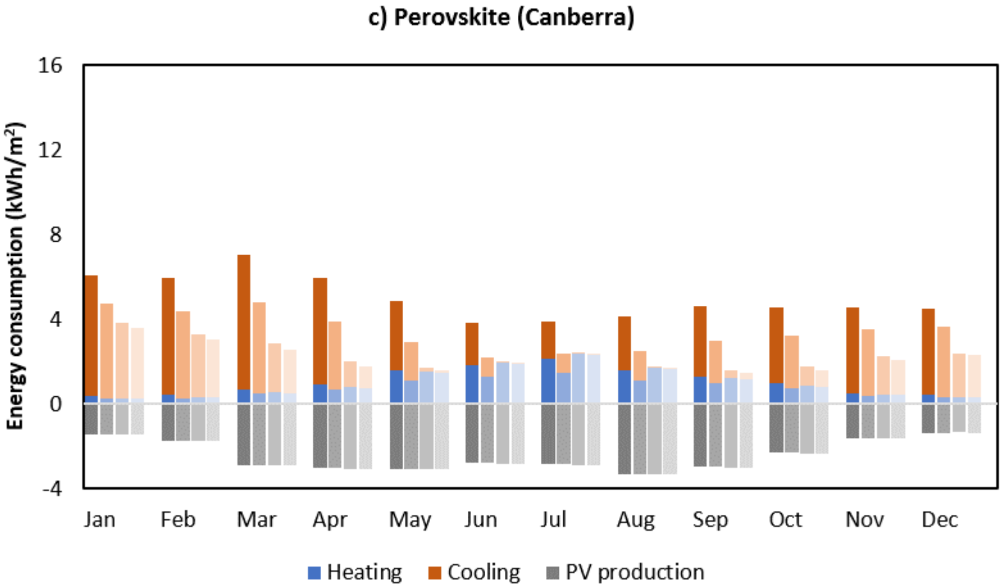

Fig. 8 a), b) and c): Energy consumption and PV production for three different PV glazing throughout the year in Canberra.

4.2 Ideal useful thermal energy

Another positive effect of BIPV/T-DSF is the availability of thermal energy generated by solar gains within the air cavity, that could be harvested at the exhaust vents. In this paragraph, the variability of the ideal useful thermal energy, calculated following the equation (1) introduced in the previous paragraphs, is described by analysing the influence of climate and of façade's type. For this analysis, only models (3) and (4) were used, since there is no direct collection of thermal energy from model (1) – single skin – and from model (2) – non-ventilated double-skin.

Fig. 9 shows the monthly collected thermal energy for models (3) and (4) located in Darwin. For both models, the production of thermal energy is concentrated in the central months of the year (May to August), and a-Si PV harvested the highest amount of thermal energy, due to the lowest solar transmittance and, therefore, the highest absorption of solar radiation and release towards the air cavity. The other two PV types show, instead comparable results. The negative values, shown during the hottest months of the year, which are possibly due to the incident solar radiation turn towards the south-facing façade (opposite the BIPV/T-DSF) of the building during the time period. Especially in mechanically ventilated air cavities, it happens that the temperature of the air within the cavity could be lower than the outside temperature, due to the heat exchange that happens between the room (with a controlled environment with low air temperatures) and the cavity. As predictable, as the collected thermal energy is a function of the air flow rate, the mechanically-ventilated model (4) provides always better performances than the naturally-ventilated one (3).

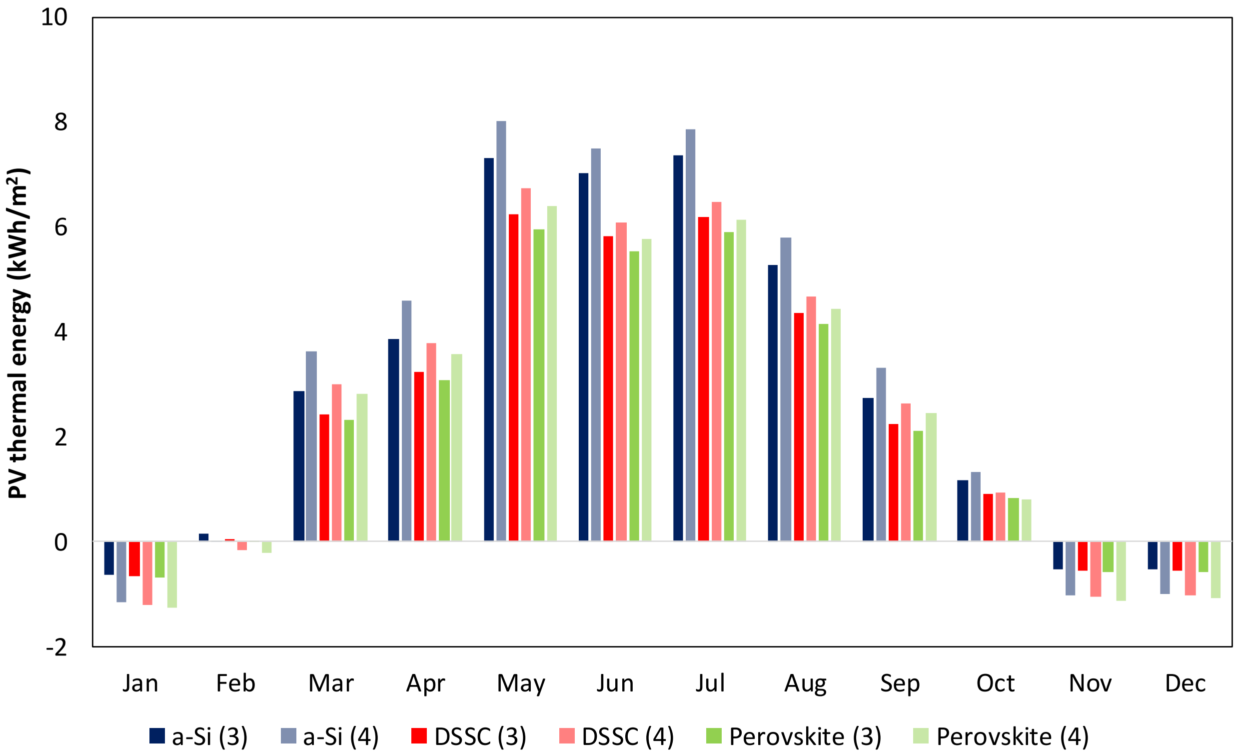

Fig. 9: Ideal useful thermal energy for three different PV/T glazing and for models (3) and (4) throughout the year in Darwin

Fig. 10 shows the monthly collected thermal energy for models (3) and (4) located in Sydney. For both models the highest production of thermal energy is concentrated in the central months of the year (between March and September). During hot months, indeed, the gradient between inlet and outlet air temperature within the air cavity is lower than the one achievable in cold and shoulder months. Among the three PV types, a-Si is still the one better performing under the thermal point of view for the reason reported above. In the case of the temperate hot climate of Sydney, it can be noticed that the difference between the performances of the two models is not as high as the one highlighted in the previous analysis in hot climates. However, it can be noticed that in all periods except the coldest months of the year (i.e. June, July and August) the mechanically-ventilated model (4) performs better than the naturally-ventilated one (3).

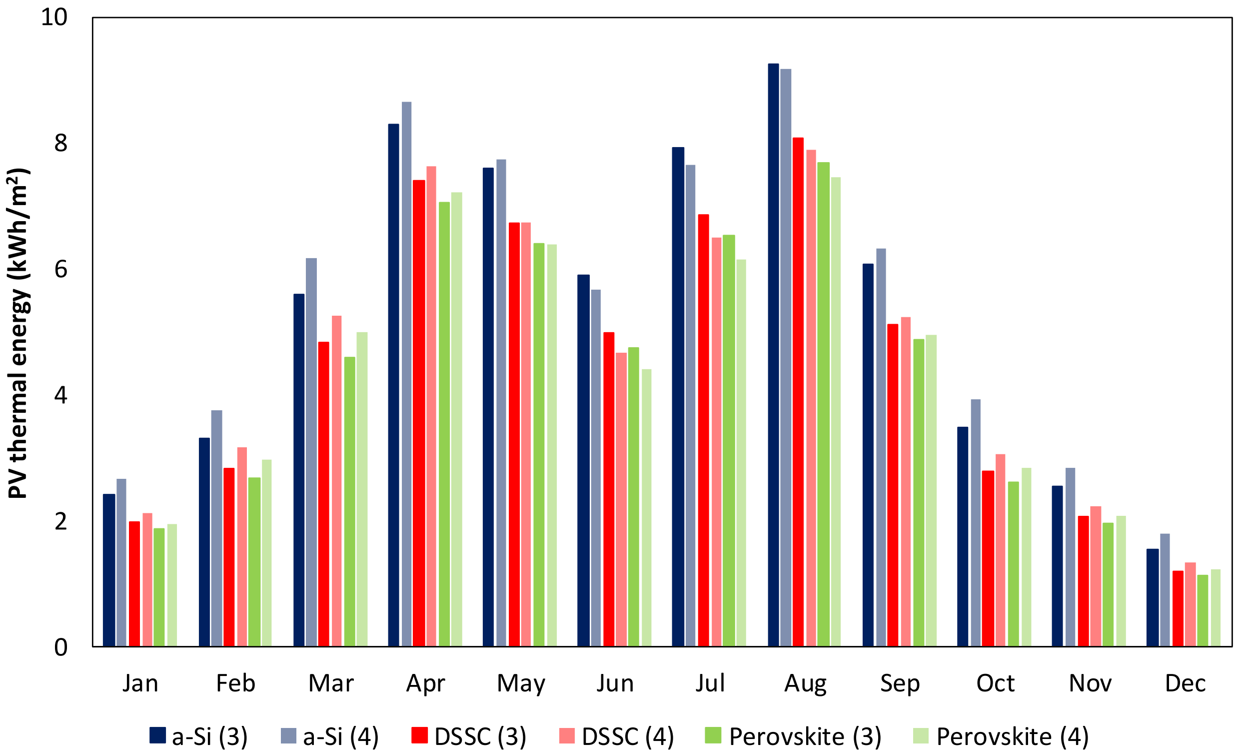

Fig. 10: Ideal useful thermal energy for three different PV/T glazing and for models (3) and (4) throughout the year in Sydney

Finally, the analysis of benefits of the mechanically-ventilated and naturally-ventilated models in terms of collected thermal energy in the cold temperate climate of Canberra is presented in Fig. 11. The results are similar to the ones obtained for the climate of Sydney, as the highest production of thermal energy is concentrated in the central months of the year (between March and September). However, in cold climate the variability of productivity between hot and cold months is limited (with the exclusion of the hottest months of December and January, the highest production of thermal energy is less than 3 times higher than the lowest one). Similarly, also the difference of thermal production between naturally-ventilated model (3) and mechanically-ventilated one (4) is limited, being still the naturally-ventilated model to be preferred only during cold months (i.e. from May to August).

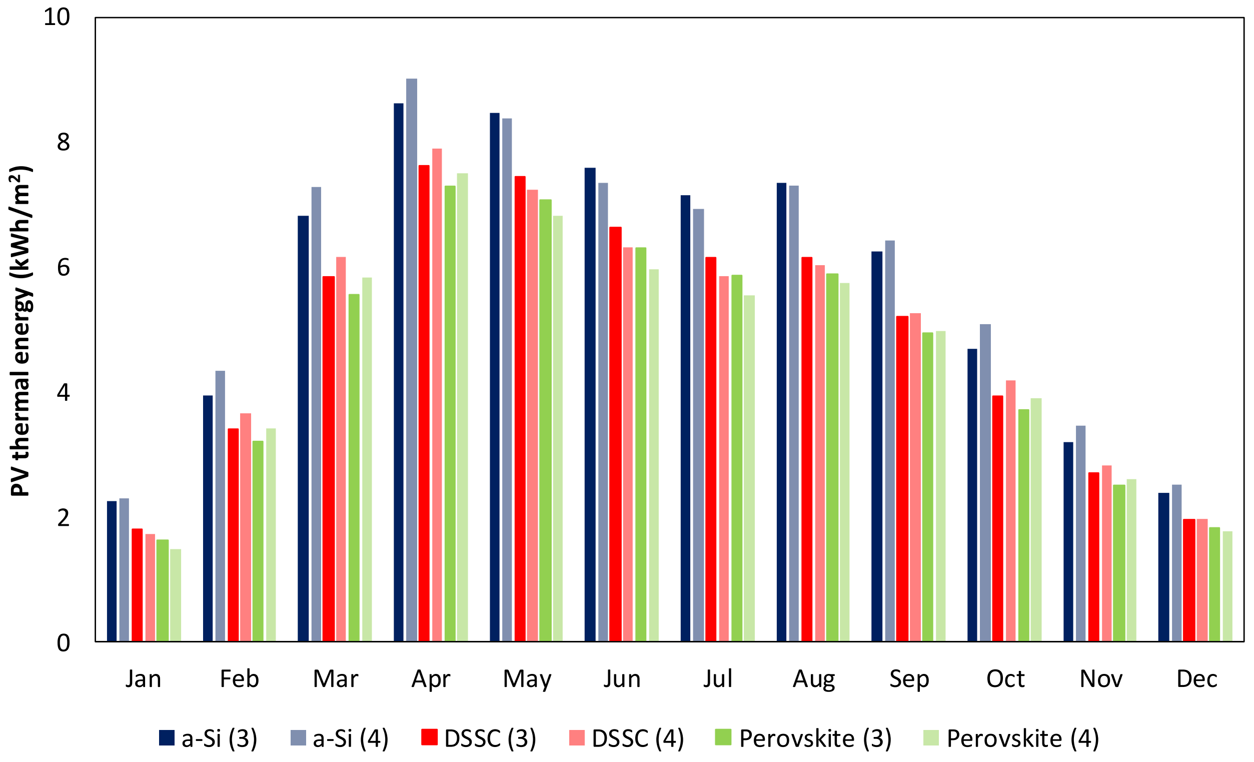

Fig. 11: Ideal useful thermal energy for three different PV/T glazing and for models (3) and (4) throughout the year in Canberra

5. Discussion

5.1 Effects on energy consumption of the BIPV/T-DSF building

The benefits in terms of reduction of the overall energy consumption of BIPV/T-DSF are reported in the current paragraph. The benefits are calculated by comparing the energy performance in terms of heating and cooling consumption and conversion of electrical energy from the PV system of DSFs (nominally models (2), models (3) and models (4) previously presented) and SSFs (nominally model (1) previously presented). In the following Fig. 12, Fig. 13, and Fig. 14 the results of the analysis performed for the three climatic areas (represented by Darwin, Sydney and Canberra) are presented. The results show the minimum and maximum percentage of variation of monthly energy data, together with the average annual variation. In Darwin (Fig. 12) the total monthly energy saving due to the adoption of a DSF instead of a SSF varies between 14.6% and 67.1%. It can be noticed that, while the minimum monthly energy saving is almost stable and independent on the DSF type and on the PV type, the maximum energy saving strongly depends on the mode of operation of DSF, where mechanically-ventilated DSF and naturally-ventilated ones perform much better than the non-ventilated types. It can be, also, noticed that the PV type affects in a significant way the energy saving, with the perovskite type which is able to reach better energy performances of the overall façade. The yearly values of energy savings vary between 22.6% and 37.2%. Also, for this performance parameter the best-performing solution is the mechanically-ventilated DFS with perovskite PV. As the total energy consumption in hot tropical climate mostly depends on the cooling energy consumption, the extreme variability of heating consumption savings – shown in Fig. 12 a) – does not affect significantly the energy performance of the façade. It can also be noticed the limited variability of PV production with PV type and DSF type. Only a 0.6% of increase of PV production is achieved by back-ventilating the PV panel.

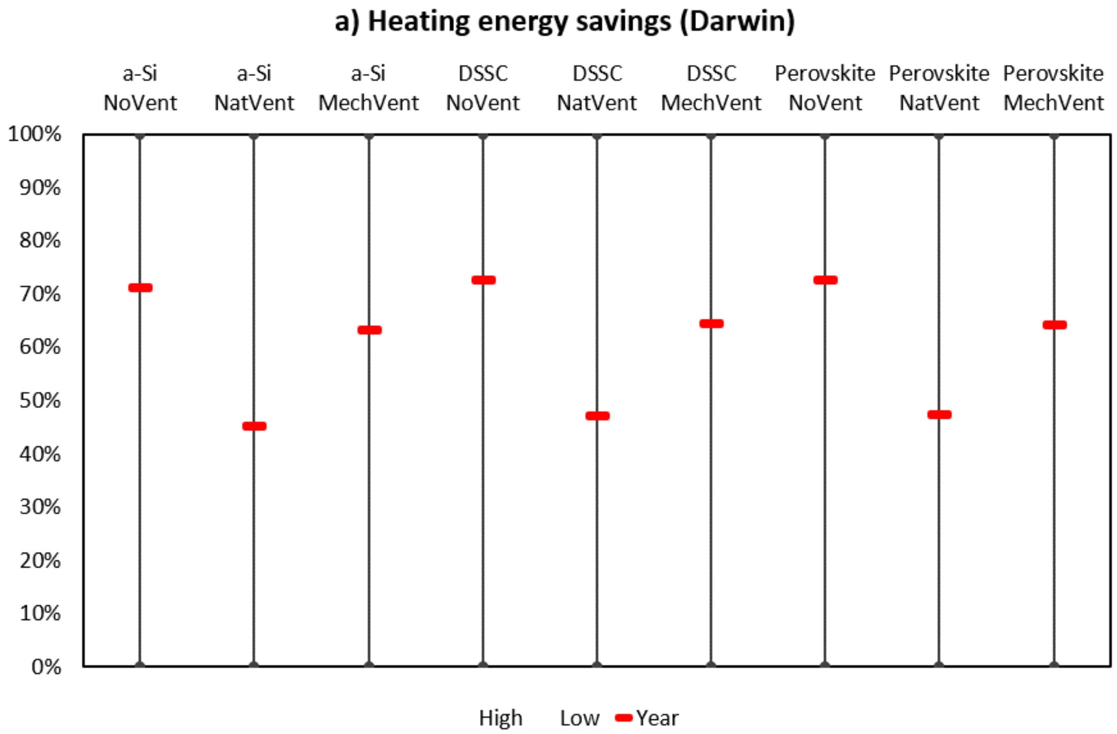

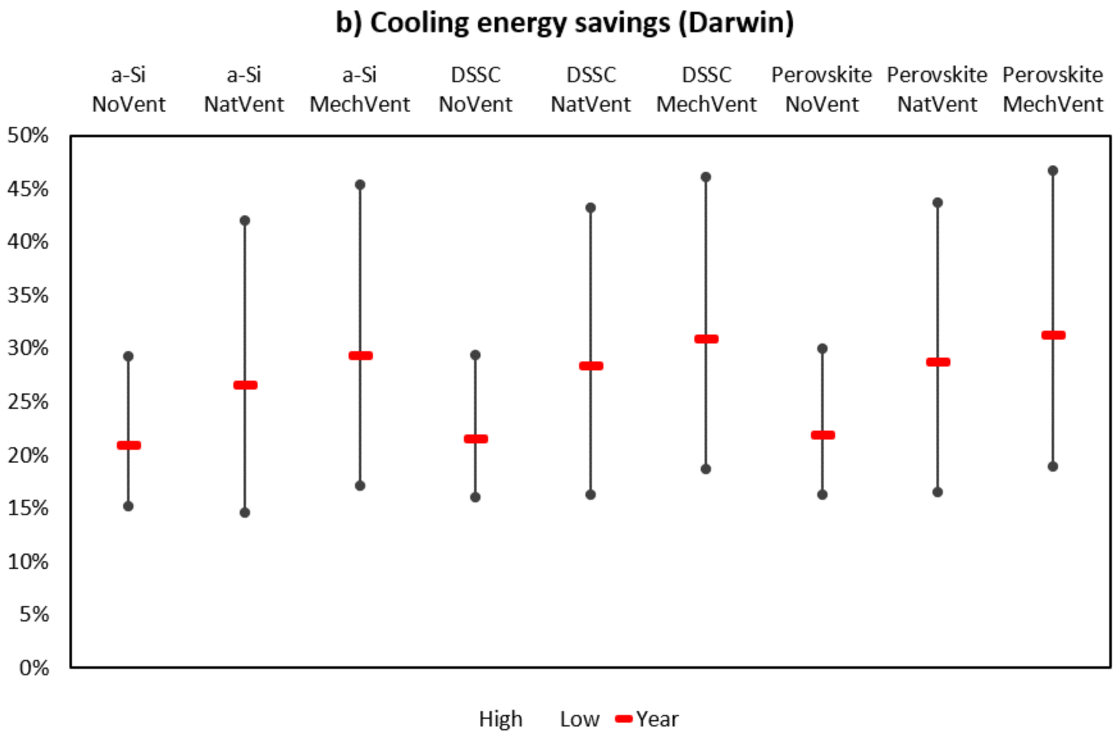

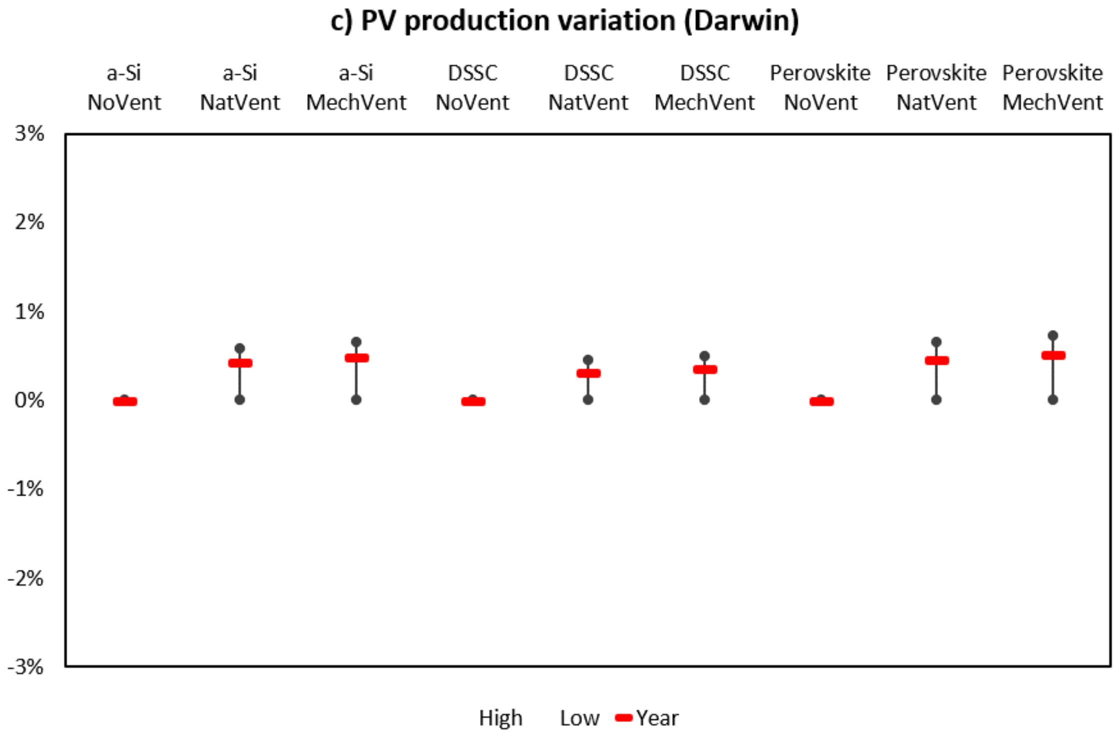

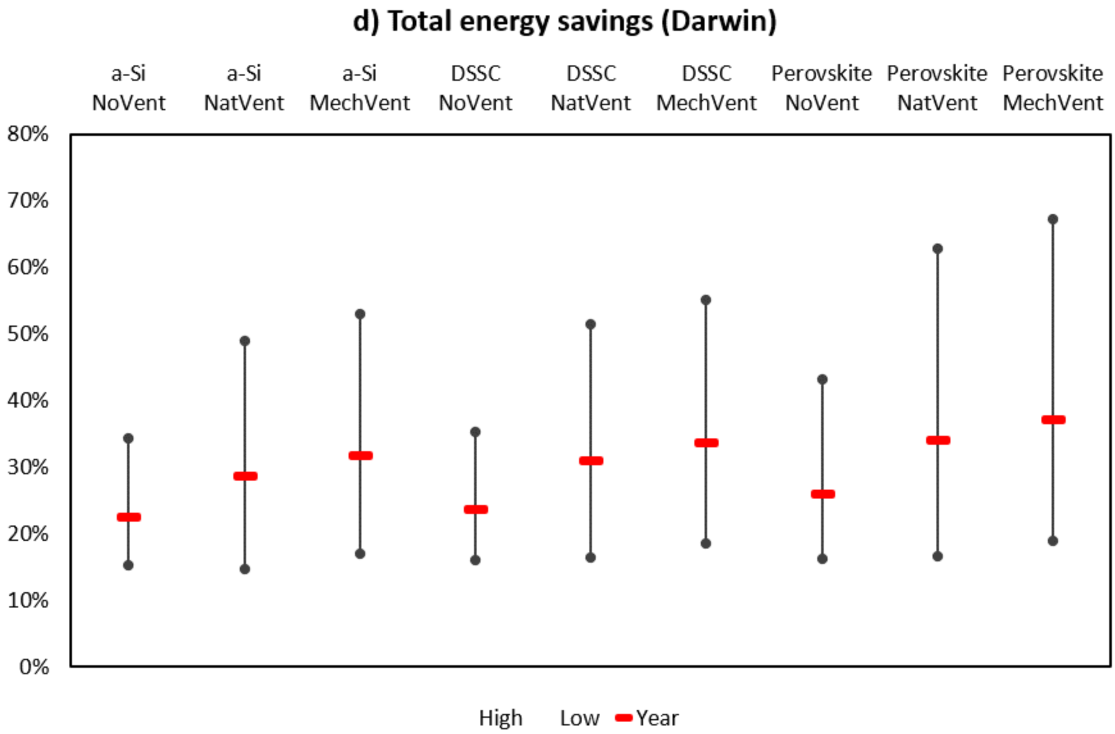

Fig. 12 a), b), c) and d): Energy savings and PV production variation for three different types of BIPV/T-DSF throughout the year in Darwin.

In Sydney (Fig. 13), the energy savings due to the reduction of the heating consumption show peaks – for both the minimum and maximum monthly values and the average annual value – for the non-ventilated BIPV/T type. It can be noticed, also, that the savings are almost independent on the PV type. On the other hand, cooling consumption benefits from ventilation, and the mechanically-ventilated solution is the most beneficial one. Conversion of solar energy into electricity by the PV system shows a limited variability but benefits from the presence of a constant back ventilation. With regards to the total energy savings, the higher amount of energy converted by perovskite solar cells, determines better performances of both naturally-ventilated and mechanically-ventilated DSFs with perovskite PV. In this case, the total yearly energy saving reaches the value of 92.1%.

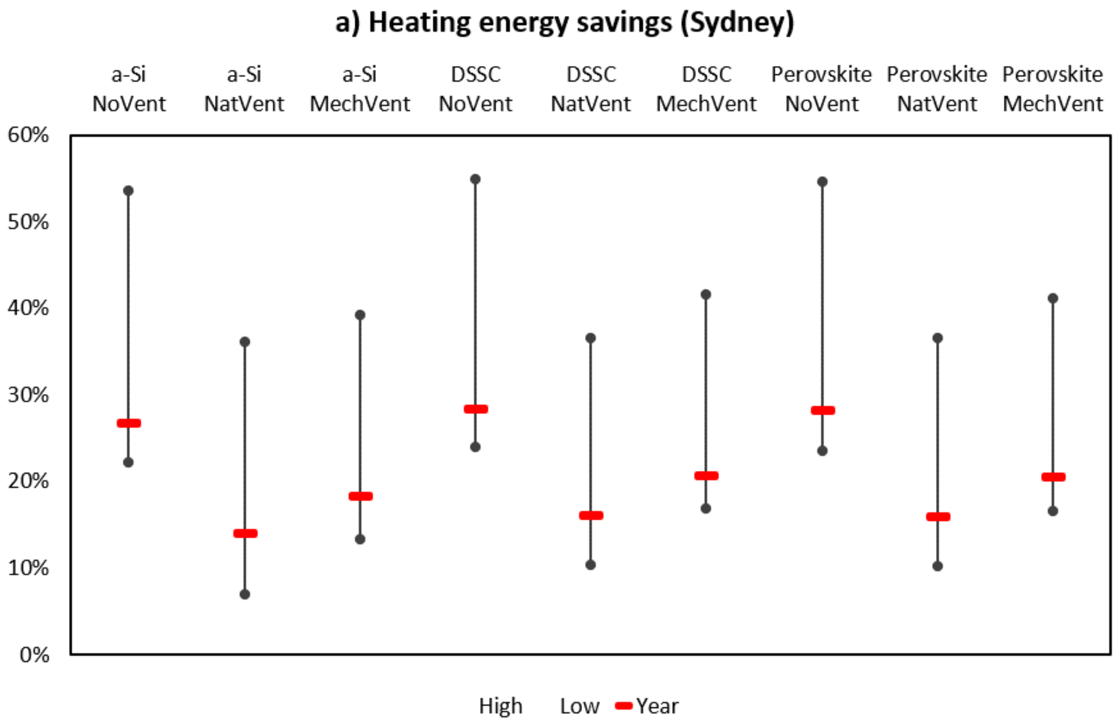

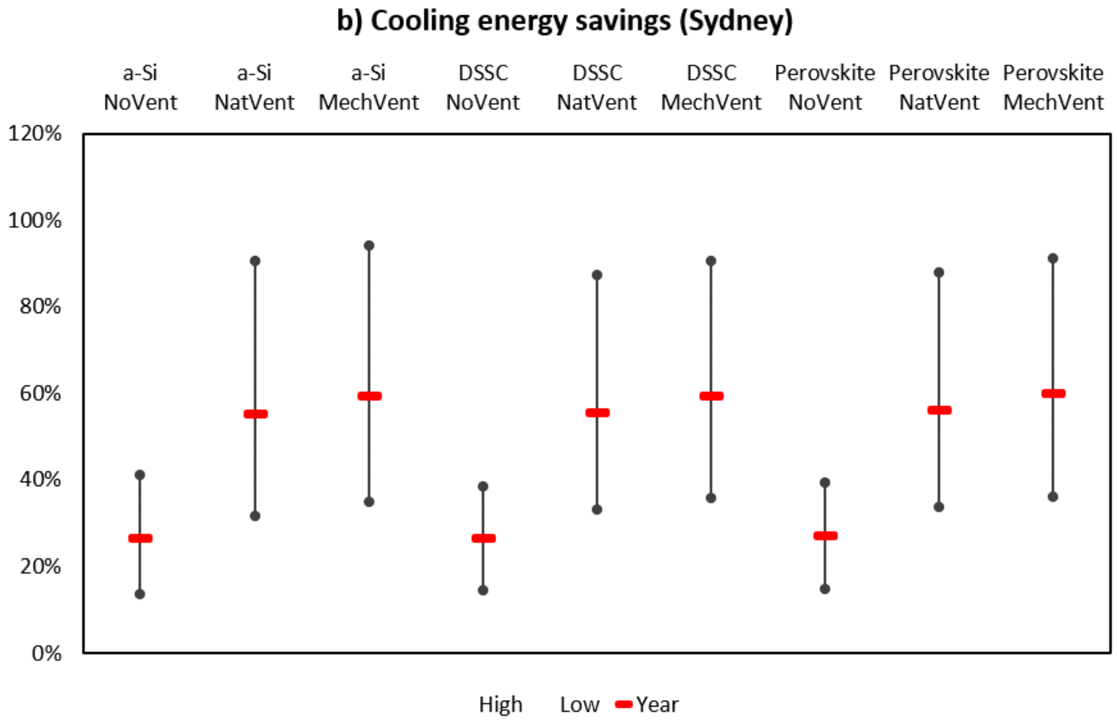
b) Cooling energy savings (Sydney)
a-Si NoVent
a-Si NatVent
a-Si MechVent
DSSC NoVent
DSSC NatVent
DSSC MechVent
Perovskite NoVent
Perovskite NatVent
Perovskite MechVent
120%
100%
80%
60%
40%
20%
0%
High
Low
Year

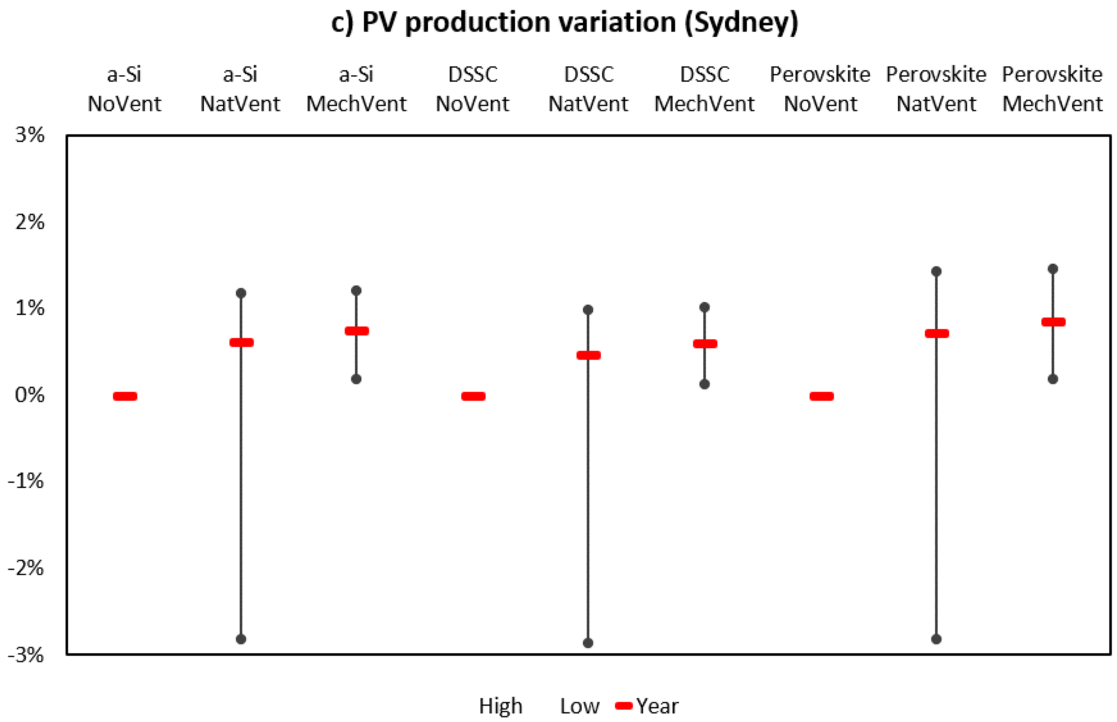
c) PV production variation (Sydney)
a-Si NoVent
a-Si NatVent
a-Si MechVent
DSSC NoVent
DSSC NatVent
DSSC MechVent
Perovskite NoVent
Perovskite NatVent
Perovskite MechVent
3%
2%
1%
0%
-1%
-2%
-3%
High
Low
Year

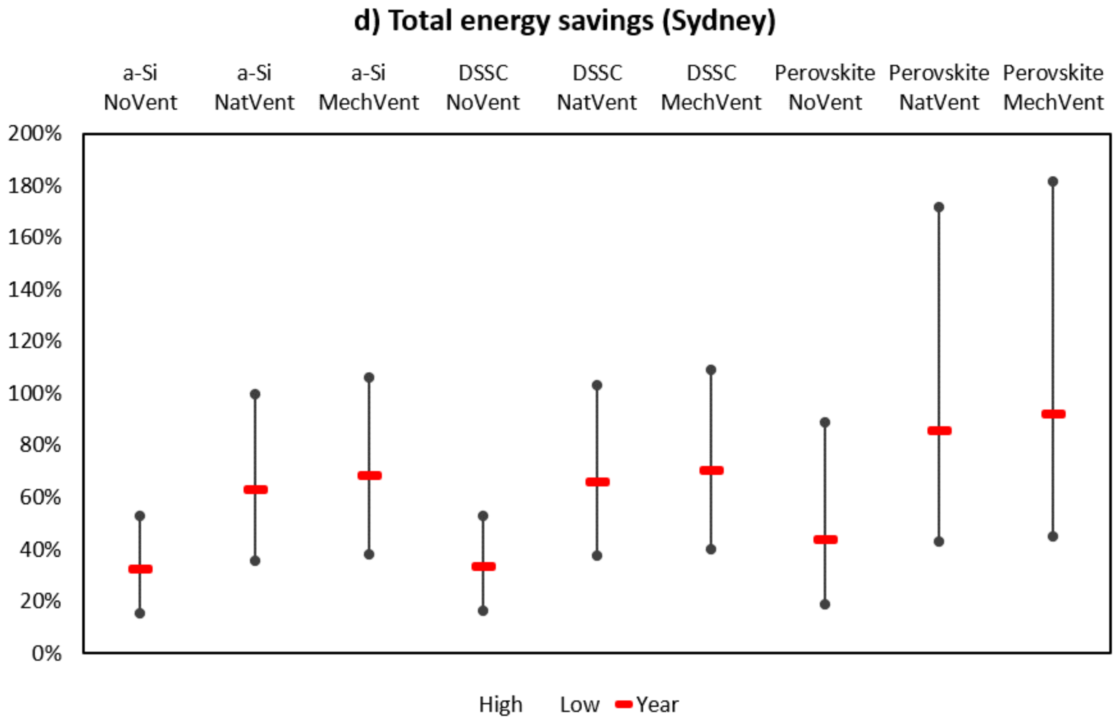

Fig. 13 a), b), c) and d): Energy savings and PV production variation for three different types of BIPV/T-DSF throughout the year in Sydney.

Finally, Fig. 14 includes the energy savings obtained by comparing the BIPV/T-DSFs in cold temperate climate (i.e. Canberra). The results show a similar trend compared to the warm temperate climate of Sydney, but with higher total energy savings. In the winter season the highest benefits are achieved with a non-ventilated DSF, independently on the PV type, while in the summer season the best-performing solutions are the ventilated ones (both naturally-ventilated and mechanically-ventilated, with the latter achieving a little bit higher performance than that of the former). Overall, on a yearly basis, due to the higher solar conversion rate of the perovskite solar cells, the solution with the highest benefits is a ventilated DSF with perovskite cells. In this last case, the yearly energy saving reaches the value of 112.9%.

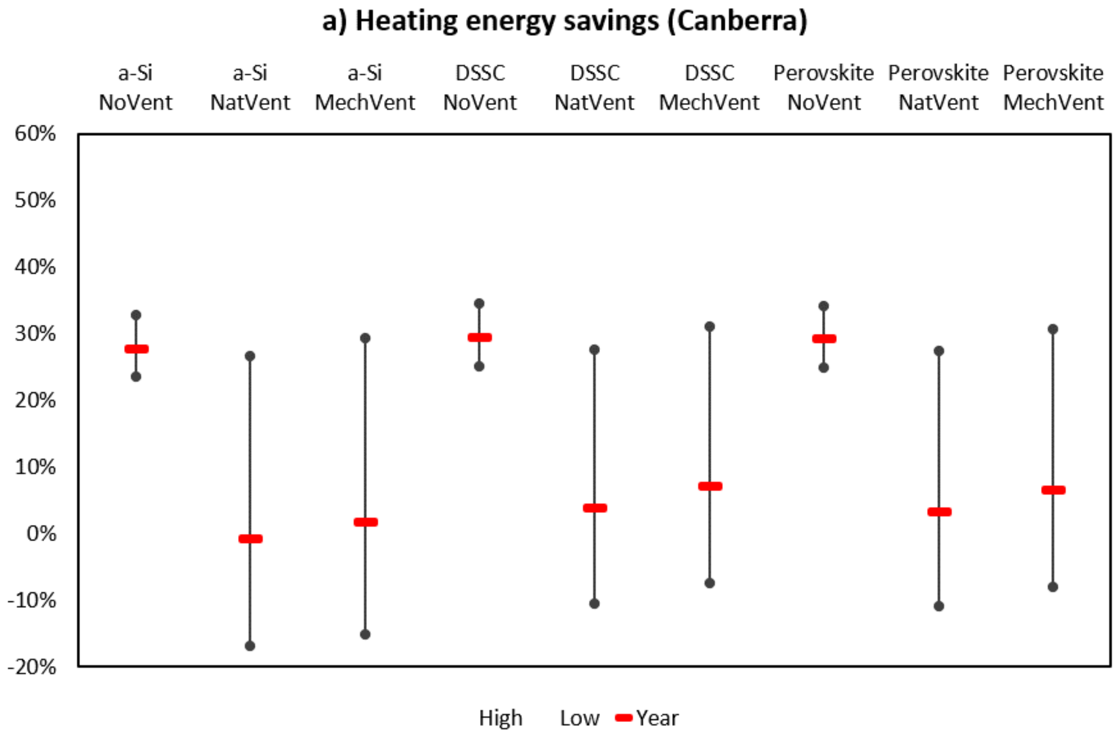
a) Heating energy savings (Canberra)
a-Si NoVent
a-Si NatVent
a-Si MechVent
DSSC NoVent
DSSC NatVent
DSSC MechVent
Perovskite NoVent
Perovskite NatVent
Perovskite MechVent
60%
50%
40%
30%
20%
10%
0%
-10%
-20%
High
Low
Year

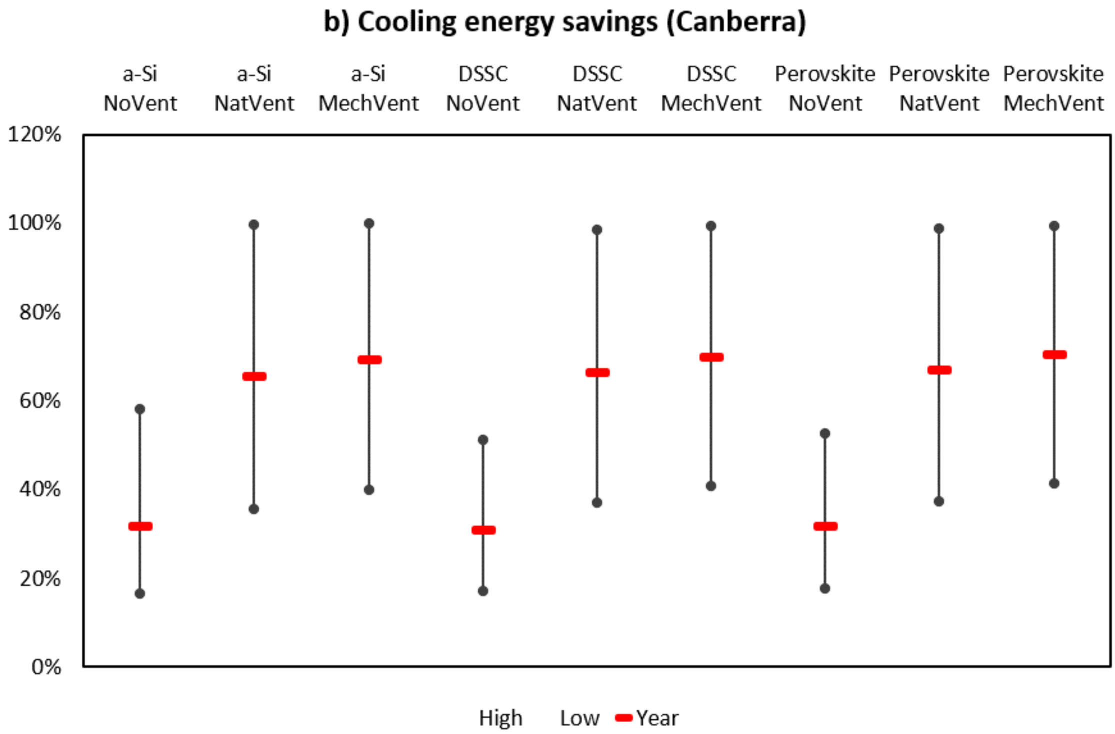
b) Cooling energy savings (Canberra)
a-Si NoVent
a-Si NatVent
a-Si MechVent
DSSC NoVent
DSSC NatVent
DSSC MechVent
Perovskite NoVent
Perovskite NatVent
Perovskite MechVent
120%
100%
80%
60%
40%
20%
0%
High
Low
Year

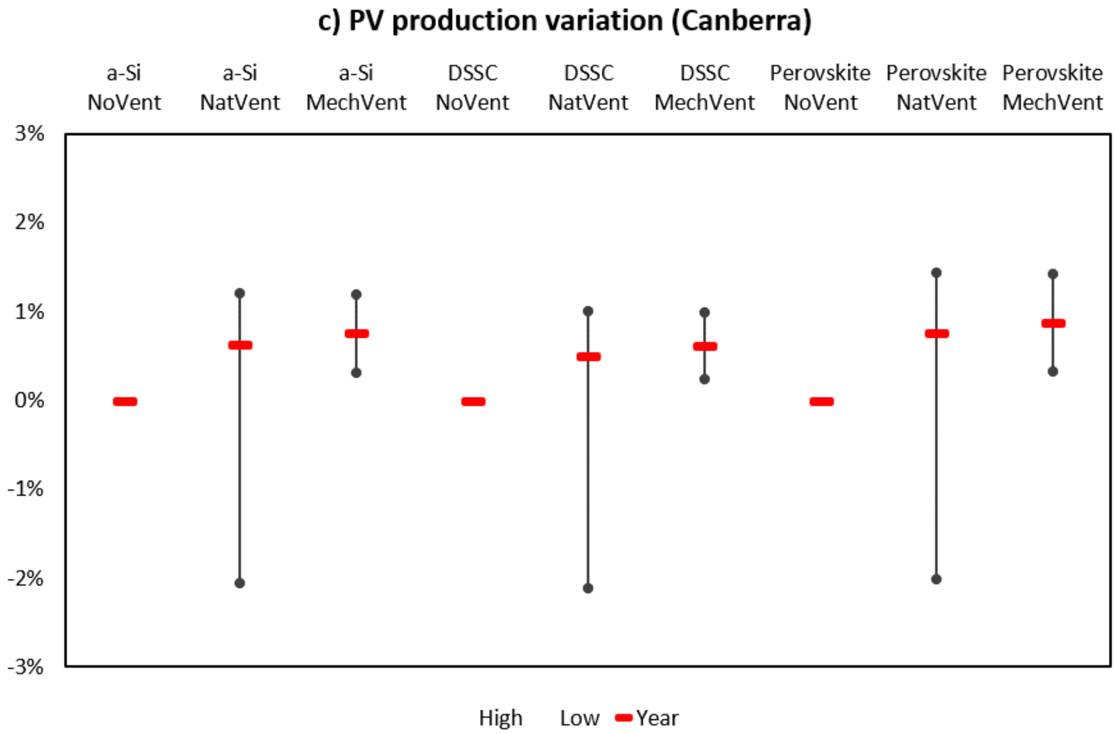

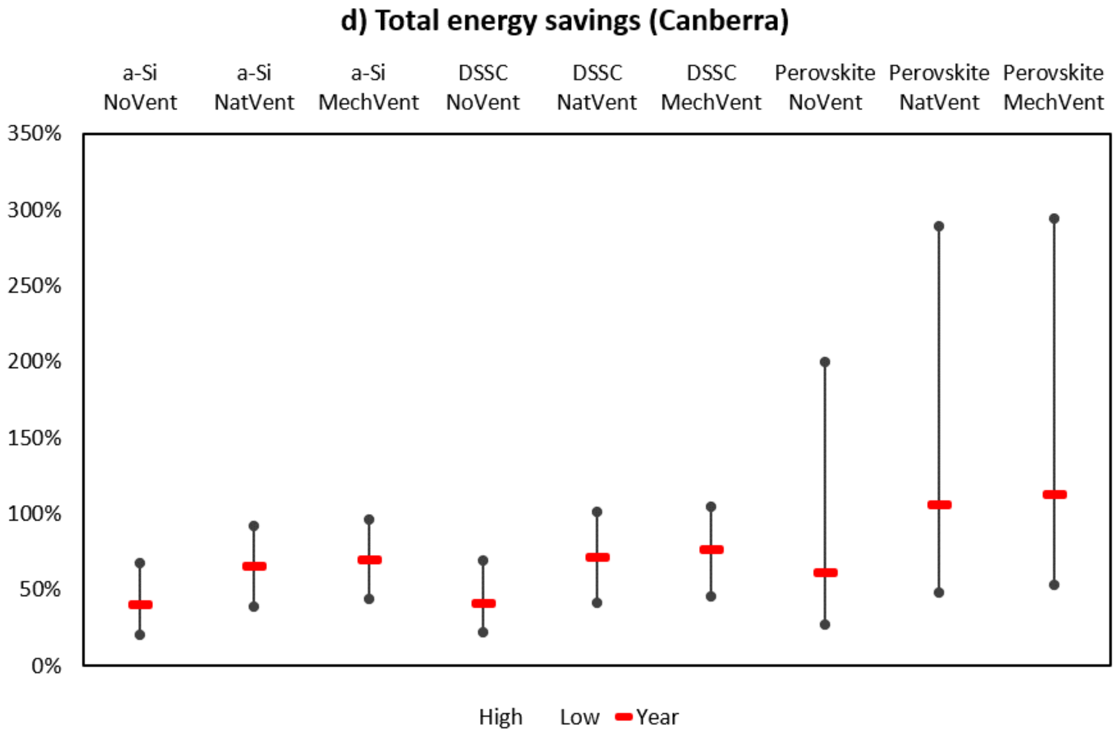

Fig. 14 a), b), c) and d): Energy savings and PV production variation for three different types of BIPV/T-DSF throughout the year in Canberra.

5.2 Comparison between useful thermal energy and heating and cooling load.

Based on the results of the simulation performed and presented in the previous paragraphs, we tried to identify benefits and limits of using the ideal thermal energy (Q) produced in the ventilated DSFs – models (3) and (4) – for providing direct heating and cooling to the internal space. The high solar conversion rate PV panel – perovskite solar cells – has been used for the analysis.

In Fig. 15 the hourly values of the useful thermal energy are plotted against the ones of heating load during the typical winter week. Only Sydney and Canberra have been considered in this analysis, since the heating load in Darwin showed values very close to zero even during the coldest days of the year. In both Sydney and Canberra it can be noticed a misalignment between production of energy (which show a peak at around 1 pm each day) and load (which has a peak at around 8-9 am). As a result, although the peaks of load and useful thermal energy are comparable, only about the 15% and 30% of the heating load respectively in Sydney and Canberra can be directly covered by the useful thermal energy. Consequently, in Sydney only about 5% of the useful thermal energy can be used to directly provide heating for the internal space, while in Canberra the percentage increases but remains close to low values (about 20%).

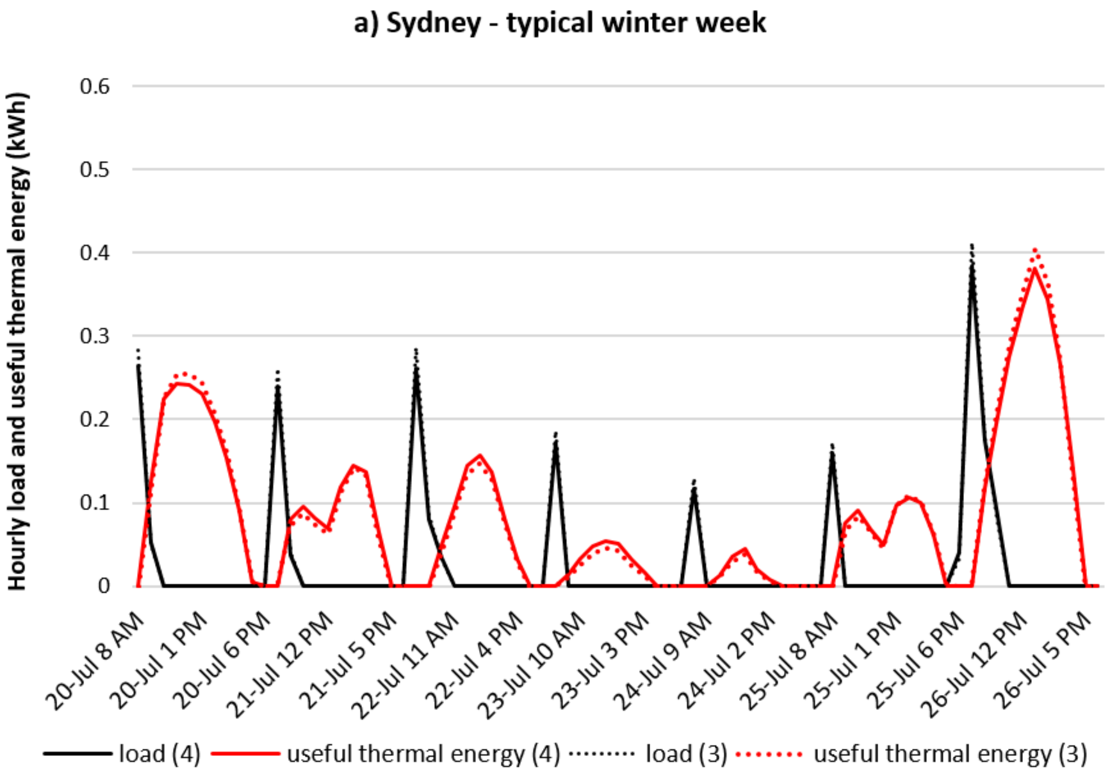

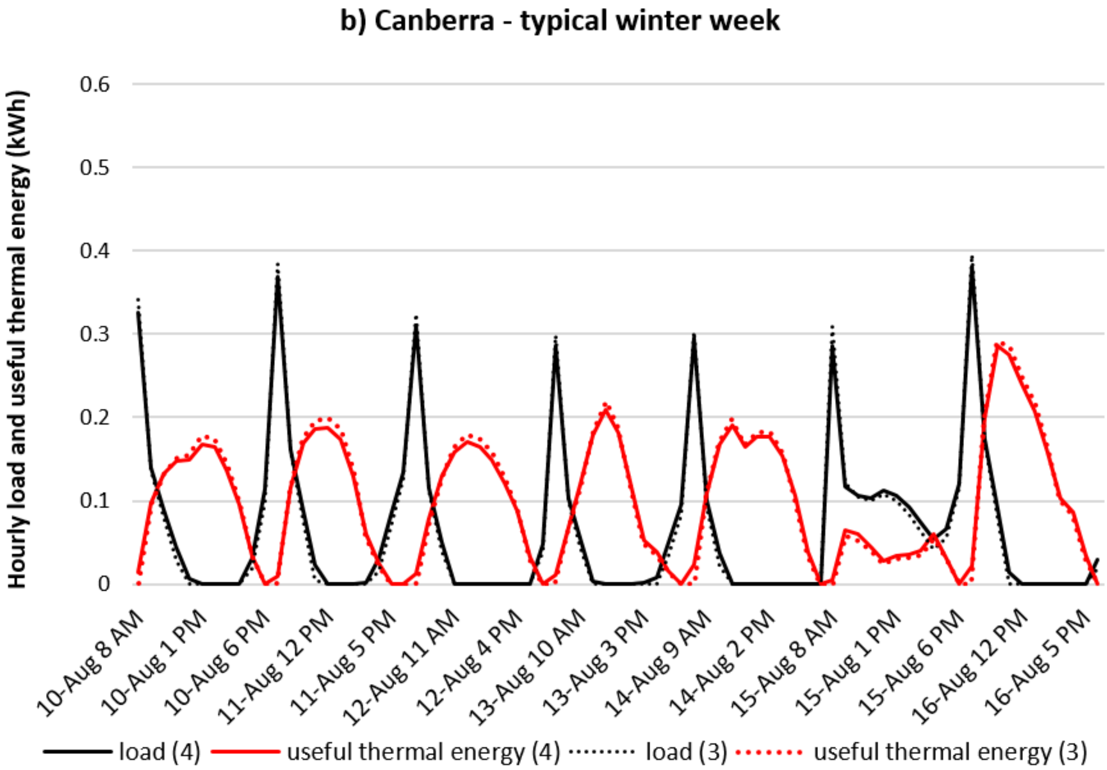

Fig. 15: Useful thermal energy against heating consumption during winter typical week in a) Sydney and b) Canberra.

Finally, it can be noticed that there is a limited difference of behaviour between the naturally-ventilated model (3) and the mechanically-ventilated one (4).

During the hot season, as illustrated in Fig. 16, the peaks of cooling load and useful thermal energy are concentrated in almost the same time range. This makes the usage of thermal energy produced within the air cavity more convenient than in the winter period. However, it can be noticed that the useful thermal energy, depending on the climate zone, is able to cover only a limited amount of the cooling load. As a result, in Darwin a cooling load reduction of 9% has been predicted, while in Sydney and Canberra the saving increases respectively to 12% and 18%. As there is an almost coincident pattern between cooling load and useful thermal energy production, in Darwin there is no waste of useful thermal energy as the whole amount of it can be directly used. In Sydney and Canberra there is still a limited amount of useful thermal energy wasted, which is approximately equal to 13% and 21% respectively.

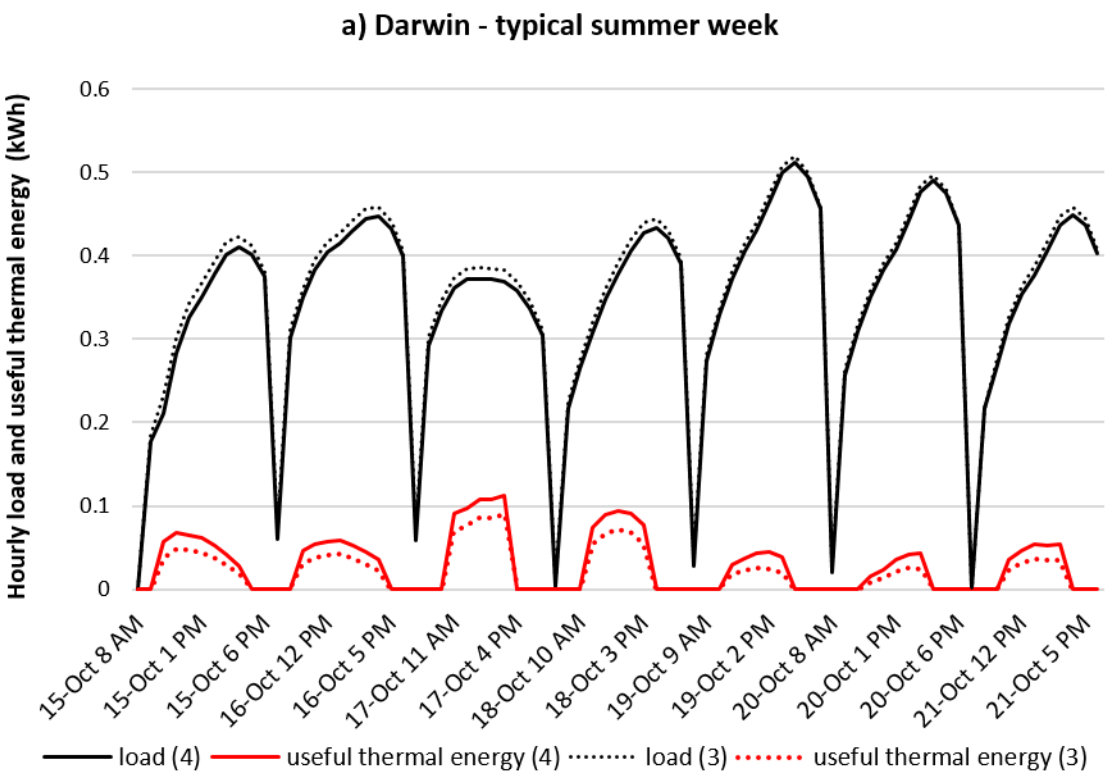
a) Darwin - typical summer week
Hourly load and useful thermal energy (kWh)
0.6
0.5
0.4
0.3
0.2
0.1
0
15-Oct 8 AM
15-Oct 1 PM
15-Oct 6 PM
16-Oct 12 PM
16-Oct 5 PM
17-Oct 11 AM
17-Oct 4 PM
18-Oct 10 AM
18-Oct 3 PM
19-Oct 9 AM
19-Oct 2 PM
20-Oct 8 AM
20-Oct 1 PM
20-Oct 6 PM
21-Oct 12 PM
21-Oct 5 PM
load (4)
useful thermal energy (4)
load (3)
useful thermal energy (3)

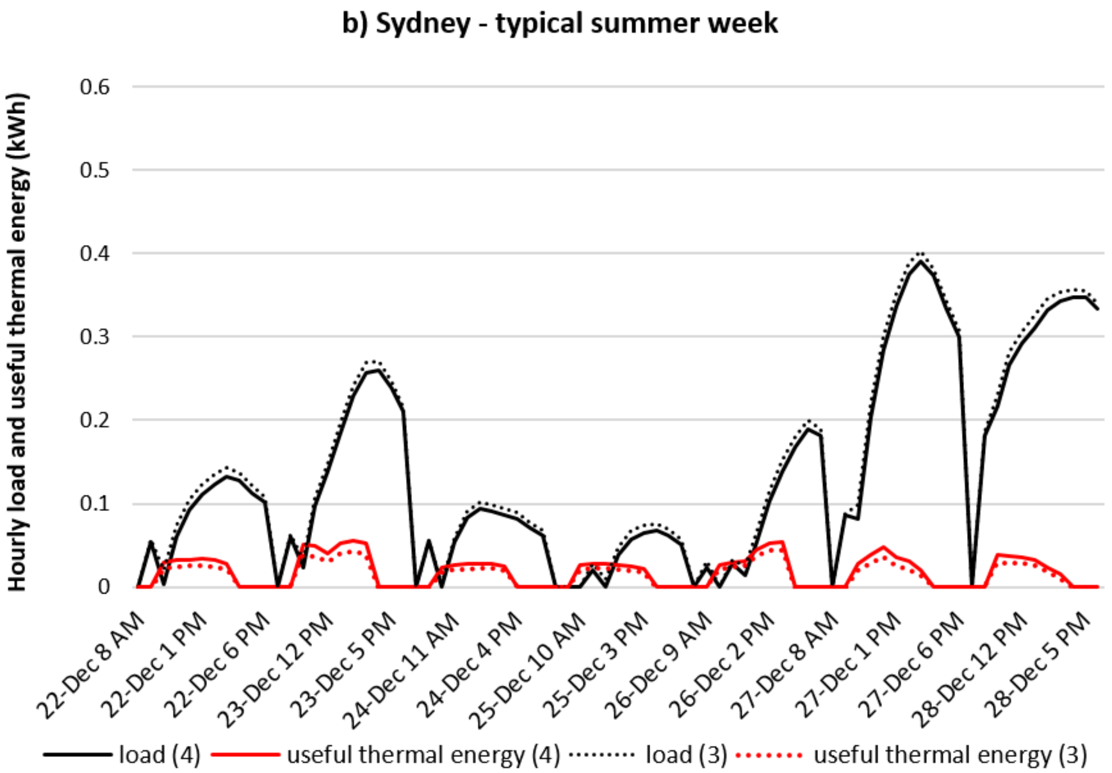
b) Sydney - typical summer week
Hourly load and useful thermal energy (kWh)
0.6
0.5
0.4
0.3
0.2
0.1
0
22-Dec 8 AM
22-Dec 1 PM
22-Dec 6 PM
23-Dec 12 PM
23-Dec 5 PM
24-Dec 11 AM
24-Dec 4 PM
25-Dec 10 AM
25-Dec 3 PM
26-Dec 9 AM
26-Dec 2 PM
27-Dec 8 AM
27-Dec 1 PM
27-Dec 6 PM
28-Dec 12 PM
28-Dec 5 PM
load (4)
useful thermal energy (4)
load (3)
useful thermal energy (3)

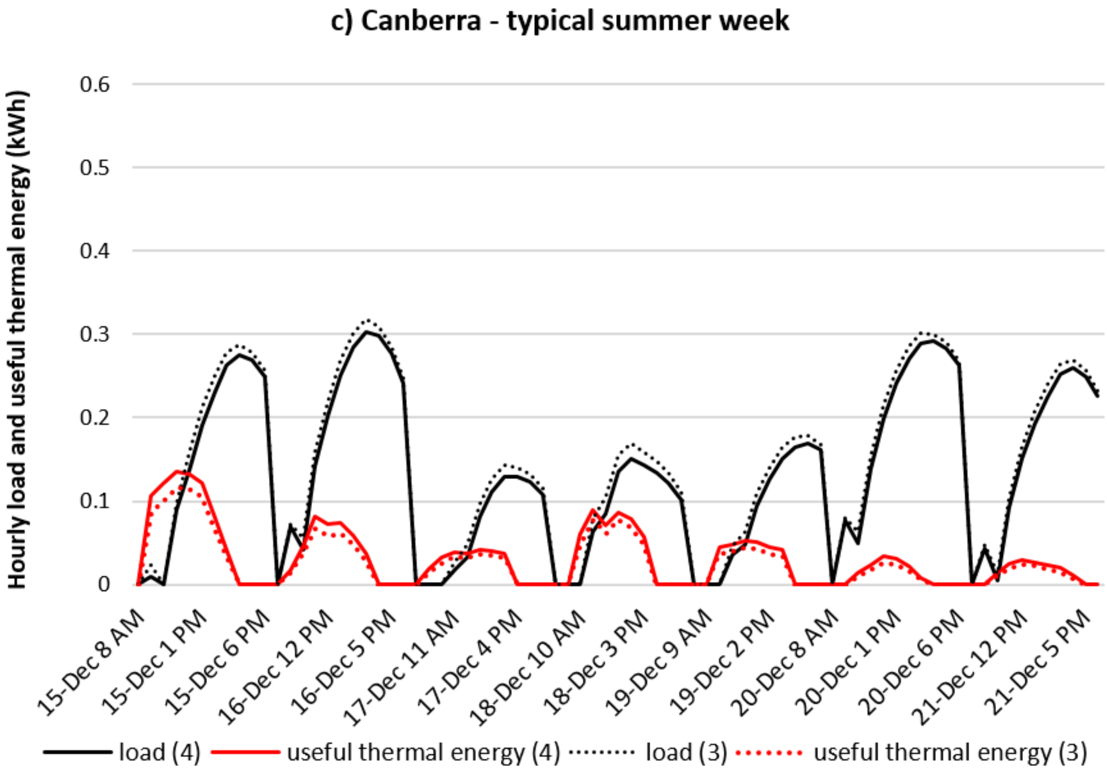

Fig. 16: Useful thermal energy against cooling consumption during summer typical week in a) Darwin, b) Sydney, and c) Canberra.

Finally, for all the three climate zones, during the summer season the mechanically-ventilated mode of operation of the air cavity ventilation has higher benefits than the naturally-ventilated one. The benefits are demonstrated both in terms of lower cooling loads (3%, 6%, and 8% lower respectively in Darwin, Sydney, and Canberra) and in terms of higher useful thermal energy production (30%, 23%, and 17% higher respectively in Darwin, Sydney, and Canberra).

6. Conclusion

In this paper, we performed a detailed assessment of energy performances of BIPV/T-DSF, by means of numerical simulations. Three types of PV glazing (a-Si, DSSC, and Perovskite-based) and three types of air-cavity ventilation modes (no ventilation, natural ventilation and mechanical ventilation) were assessed. The cooling and heating energy consumption was predicted with reference to three cities (i.e. Darwin, Sydney and Canberra), representative of as many Australian climate zones, from hot humid to cool temperate. An office building was considered as case study. The major findings can be summarized as follows:

1. The model with an air cavity with ventilation mechanically-controlled shows the lowest cooling energy consumption. This evidence is valid for all the three climate zones and independently from the PV type used. Moreover, for both warm temperate (Sydney) and cool temperate (Canberra) climate zones, a DSF with non-ventilated air cavity shows the lowest heating energy consumption.

2. The façade equipped with Perovskite-based solar cells is the one able to convert the highest amount of solar radiation into electricity, due to its high power efficiency (6.64%). The electricity production is not significantly affected by the ventilation mode of the air cavity (about 1% difference moving from non-ventilated air cavity to ventilated one).
3. For hot humid climate (Darwin), the highest yearly amount of the total energy savings reaches the value of 37.2%. In this case the best-performing façade typology is the mechanically-ventilated one. Moreover, for warm temperate climate (Sydney) and the cool temperate one (Canberra) the highest amount of total yearly energy savings reaches the values of respectively 92.1% and 112.9%. As for the hot humid climate, the best-performing façade typology is the mechanically-ventilated one, even though there are limited differences with the naturally-ventilated one.
4. Both the naturally-ventilated and the mechanically-ventilated DSFs are able to collect useful thermal energy, with the highest peak of production concentrated in the winter season, due to the higher temperature difference between the DSF and the outdoor. However, there is a lag between the peak of production of useful thermal energy (use the perovskite solar cells as the case study) and the peak of required thermal load and, consequently, only a limited amount of useful thermal energy (5% in Sydney and 20% in Canberra) could be used to directly reduce heating load of internal spaces.
5. During summer, the collected used thermal energy could be converted in cooling energy by means of a desiccant cooling system. As the peak of production of collected thermal energy (use the perovskite solar cells as the case study) is close to the peak of cooling load, a high fraction (from 87% to 100% depending on the climate zone considered) of the collected thermal energy could be directly used. Therefore, an additional energy saving of respectively 9%, 12%, and 18% (in Darwin, Sydney, and Canberra) has been predicted.

In summary, in hot climatic conditions, and therefore in Darwin throughout the year and in Sydney and Canberra during the summer season, the double-skin façade operates better when it is mechanically ventilated. In these conditions, the PV panel with highest benefits under an energy point of view is the one based on perovskite. On the other side, in colder temperature conditions (month of July in Sydney and Canberra), the benefit due to the ventilation of the air cavity is not always as high as expected. Overall the best-performing mode of operation is the mechanically-ventilated one, but the one giving the highest contribution of reduction of heating loads is the non-ventilated one. In these climatic conditions, in analogy with the previous results, the PV panel with the highest benefit is the perovskite-based one.

Finally, it has to be highlighted that, although the study has focused on the effects under an energy point of view of integrating BIPV-DSFs into buildings considering as main variables the PV type and the DSF mode of operation, from the sensitivity analysis performed, it has been highlighted that other parameters, such as internal window's thermal transmittance, cavity depth, opening ratio of ventilation louvres, and airflow rate of mechanically-ventilated operational mode could significantly affect the façade performance. All these parameters will be the focus of the future studies.

References

1. Pérez-Lombard, L., J. Ortiz, and C. Pout, *A review on buildings energy consumption information.* Energy and Buildings, 2008. **40**(3): p. 394-398.
2. Synnefa, A., M. Santamouris, and H. Akbari, *Estimating the effect of using cool coatings on energy loads and thermal comfort in residential buildings in various climatic conditions.* Energy and Buildings, 2007. **39**(11): p. 1167-1174.
3. Ernst & Young, *Mid-tier commercial office buildings in Australia*. 2015.
4. Council of Australian Governments, *Baseline Energy Consumption and Greenhouse Gas Emissions in Commercial Buildings in Australia (Part 1)*. 2012, Department of Climate Change and Energy Efficiency: Canberra.
5. Peng, J., et al. *182: Investigation on the overall energy performance of an a-si based photovoltaic double-skin facade in Hong Kong*. in *Proceedings of the 14th International Conference on Sustainable Energy Technologies*. 2015. Nottingham, UK.
6. Halawa, E., et al., *A review on energy conscious designs of building façades in hot and humid climates: Lessons for (and from) Kuala Lumpur and Darwin.* Renewable and Sustainable Energy Reviews, 2018. **82**: p. 2147-2161.
7. Lee, E., et al., *High-performance commercial building façades*. 2002, Lawrence Berkeley National Laboratory.
8. Shameri, M.A., et al., *Perspectives of double skin façade systems in buildings and energy saving.* Renewable and Sustainable Energy Reviews, 2011. **15**(3): p. 1468-1475.
9. Ding, W., Y. Hasemi, and T. Yamada, *Natural ventilation performance of a double-skin façade with a solar chimney.* Energy and Buildings, 2005. **37**(4): p. 411-418.
10. Gratia, E. and A. De Herde, *Optimal operation of a south double-skin facade.* Energy and Buildings, 2004. **36**(1): p. 41-60.
11. Xu, L. and T. Ojima, *Field experiments on natural energy utilization in a residential house with a double skin façade system.* Building and Environment, 2007. **42**(5): p. 2014-2023.
12. Ballestini, G., et al., *Possibilities and limitations of natural ventilation in restored industrial archaeology buildings with a double-skin façade in Mediterranean climates.* Building and Environment, 2005. **40**(7): p. 983-995.
13. Yılmaz, Z. and F. Çetintaş, *Double skin façade's effects on heat losses of office buildings in Istanbul.* Energy and Buildings, 2005. **37**(7): p. 691-697.
14. Saelens, D., J. Carmeliet, and H. Hens, *Energy Performance Assessment of Multiple-Skin Facades.* HVAC&R Research, 2003. **9**(2): p. 167-185.
15. Chan, A.L.S., et al., *Investigation on energy performance of double skin façade in Hong Kong.* Energy and Buildings, 2009. **41**(11): p. 1135-1142.
16. Prieto, A., et al., *COOLFACADE: State-of-the-art review and evaluation of solar cooling technologies on their potential for façade integration.* Renewable and Sustainable Energy Reviews, 2019. **101**: p. 395-414.
17. Yang, T. and A.K. Athienitis, *A review of research and developments of building-integrated photovoltaic/thermal (BIPV/T) systems.* Renewable and Sustainable Energy Reviews, 2016. **66**: p. 886-912.
18. Agathokleous, R.A. and S.A. Kalogirou, *Double skin facades (DSF) and building integrated photovoltaics (BIPV): A review of configurations and heat transfer characteristics.* Renewable Energy, 2016. **89**: p. 743-756.
19. Buonomano, A., et al., *BIPVT systems for residential applications: An energy and economic analysis for European climates.* Applied Energy, 2016. **184**: p. 1411-1431.
20. Guarracino, I., et al., *Systematic testing of hybrid PV-thermal (PVT) solar collectors in steady-state and dynamic outdoor conditions.* Applied Energy, 2019: p. 1014-1030.
21. Kuo, C.F.J., et al., *A bifacial photovoltaic thermal system design with parameter optimization and performance beneficial validation.* Applied Energy, 2019. **247**: p. 335-349.
22. Agathokleous, R., et al., *Building façade integrated solar thermal collectors for air heating: experimentation, modelling and applications.* Applied Energy, 2019: p. 658-679.

23. Asaee, S.R., et al., *Techno-economic assessment of photovoltaic (PV) and building integrated photovoltaic/thermal (BIPV/T) system retrofits in the Canadian housing stock.* Energy and Buildings, 2017. **152**: p. 667-679.
24. Delisle, V. and M. Kummert, *Cost-benefit analysis of integrating BIPV-T air systems into energy-efficient homes.* Solar Energy, 2016. **136**: p. 385-400.
25. Wang, Z., et al., *Experimental investigation of the thermal and electrical performance of the heat pipe BIPV/T system with metal wires.* Applied Energy, 2016. **170**: p. 314-323.
26. Bigaila, E., et al., *A Study of a BIPV/T Collector Prototype for Building Façade Applications.* Energy Procedia, 2015. **78**: p. 1931-1936.
27. Hassani, S., et al., *Environmental and exergy benefit of nanofluid-based hybrid PV/T systems.* Energy Conversion and Management, 2016. **123**: p. 431-444.
28. Li, S., et al., *System identification and model-predictive control of office buildings with integrated photovoltaic-thermal collectors, radiant floor heating and active thermal storage.* Solar Energy, 2015. **113**: p. 139-157.
29. Liang, R., et al., *Experiment research of solar PV/T cogeneration system on the building façade driven by a refrigerant pump.* Energy, 2018. **161**: p. 744-752.
30. Saadon, S., et al., *Simulation study of a naturally-ventilated building integrated photovoltaic/thermal (BIPV/T) envelope.* Renewable Energy, 2016. **87**: p. 517-531.
31. Joe, J., et al., *Load characteristics and operation strategies of building integrated with multi-story double skin facade.* Energy and Buildings, 2013. **60**: p. 185-198.
32. Peng, J., et al., *Investigation on the annual thermal performance of a photovoltaic wall mounted on a multi-layer façade.* Applied Energy, 2013. **112**: p. 646-656.
33. Peng, J., et al., *Numerical investigation of the energy saving potential of a semi-transparent photovoltaic double-skin facade in a cool-summer Mediterranean climate.* Applied Energy, 2016. **165**: p. 345-356.
34. Ioannidis, Z., et al., *Modeling of double skin façades integrating photovoltaic panels and automated roller shades: Analysis of the thermal and electrical performance.* Energy and Buildings, 2017. **154**: p. 618-632.
35. Peng, J., et al., *Comparative study of the thermal and power performances of a semi-transparent photovoltaic façade under different ventilation modes.* Applied Energy, 2015. **138**: p. 572-583.
36. Elarga, H., et al., *Thermal and electrical performance of an integrated PV-PCM system in double skin façades: A numerical study.* Solar Energy, 2016. **136**: p. 112-124.
37. Peng, J., L. Lu, and H. Yang, *An experimental study of the thermal performance of a novel photovoltaic double-skin facade in Hong Kong.* Solar Energy, 2013. **97**: p. 293-304.
38. Yang, S., et al., *Studies on Optimal Application of Building Integrated Photovoltaic/Thermal Facade for Commercial Buildings in Australia*, in *Solar World Congress 2017*. 2017: Abu Dhabi.
39. Yang, S., et al., *Study of Building Integrated Photovoltaic/Thermal Double-Skin Facade for Commercial Buildings in Sydney, Australia*, in *Final conference of COST TU1403 "Adaptive Facades Network"*. 2018: Lucerne, accepted.
40. Australian Building Codes Board, *National Construction Code Volume One*, in *Building Code of Australia, Class 2 to Class 9 Buildings*. 2016, Australian Building Codes Board: Canberra.
41. Architectural Louvers, *Model: E4WS Louver Performance Data*. 2010.
42. Haase, M., F. Wong, and A. Amato, *Double–Skin Facades for Hong Kong.* Surveying and Built Environment, 2007. **18**(2): p. 17-32.
43. Duffie, J.A. and W.A. Beckman, *Solar engineering of thermal processes*. 2013: John Wiley & Sons.
44. Ma, Y., et al., *Parametric Analysis of Design Parameter Effects on the Performance of a Solar Desiccant Evaporative Cooling System in Brisbane, Australia.* Energies, 2017. **10**(7).
45. Boyce, P., et al., *Minimum acceptable transmittance of glazing.* Lighting Research and Technology, 1995. **27**(3): p. 145-152.
46. Cannavale, A., et al., *Building integration of semitransparent perovskite-based solar cells: Energy performance and visual comfort assessment.* Applied Energy, 2017. **194**: p. 94-107.
47. Cannavale, A., et al., *Improving energy and visual performance in offices using building integrated perovskite-based solar cells: A case study in Southern Italy.* Applied Energy, 2017. **205**: p. 834-846.

48. Reale, A., et al., *Estimation of Energy Production of Dye-Sensitized Solar Cell Modules for Building-Integrated Photovoltaic Applications.* Energy Technology, 2014. **2**(6): p. 531-541.
49. Beckman, W.A., et al., *TRNSYS The most complete solar energy system modeling and simulation software.* Renewable Energy, 1994. **5**(1-4): p. 486-488.
50. Elarga, H., A. Zarrella, and M. De Carli, *Dynamic energy evaluation and glazing layers optimization of façade building with innovative integration of PV modules.* Energy and Buildings, 2016. **111**: p. 468-478.
51. Kamel, R.S. and A.S. Fung, *Modeling, simulation and feasibility analysis of residential BIPV/T+ASHP system in cold climate—Canada.* Energy and Buildings, 2014. **82**: p. 758-770.
52. Yang, S., et al., *Numerical simulation study of BIPV/T double-skin facade for various climate zones in Australia: Effects on indoor thermal comfort.* Building Simulation, 2019. **12**(1): p. 51-67.
53. Weber, A., et al. *TRNFLOW: Integration of COMIS into TRNSYS TYPE 56*. in *Proceedings of the 3rd european conference on energy performance and indoor climate, EPIC 2002*. 2002.
54. Favoino, F., et al., *Optimal control and performance of photovoltachromic switchable glazing for building integration in temperate climates.* Applied Energy, 2016. **178**: p. 943-961.
55. ASHRAE, *Guideline 14-2002*, in *Measurement of Energy and Demand Savings*. 2002, American Society of Heating, Refrigerating, and Air Conditioning Engineers: Atlanta, Georgia.